AN ABSTRACT OF THE THESIS OF

Satomi Harada for the Master of Science

in Physical Science presented on November 16, 2011

Title: Chemical and Physical Properties of Biodiesel

Abstract Approval:

Although biodiesel is a promising alternative fuels, it still has many challenging issues. One of the problems is its purification process. The traditional wet washing method can increase the production costs so it is important to investigate other reusable and inexpensive purifications methods. In this study, calcium-based desiccants and molecular sieves were investigated as new purification materials. The study showed that the calcium-based desiccants were comparable to wet wash purification for removing volatile byproducts; however, calcium concentration in biodiesel increased dramatically after the treatment. The application of the molecular sieves successfully achieved the reduction of calcium concentration but further experiments will be necessary to determine whether the combination of desiccants can be the replacement for the traditional purification process.

In addition, the application of biodiesel is limited due to its poor cold weather properties. In order to improve performance in the cold climate, additives are typically added to biodiesel. The second part of this study focused on the chemical and physical effects on biodiesel using various additives. Results indicated that additives can improve cold weather properties but canola oil, soybean oil, palm oil, and lard based biodiesel with 2 weight-percent of Wintron XC30 and XC40 additives could not achieve the

viscosity requirement therefore those additives were not applicable with that concentration. Also, no changes in the chemical structures and freezing point by additives were observed. A faster and novel cloud point analytical methodology using Rayleigh light scattering was developed and applied in this study.

# Chemical and Physical Properties of Biodiesel

---

A Thesis

Presented to

the Department of Physical Sciences

EMPORIA STATE UNIVERSITY

---

In Partial Fulfillment

of the Requirements for the Degree

Master Science

---

by

Satomi Harada

December 2011

Approved by the Department Chair

Committee Member

Committee Member

Committee Member

Committee Chair

Dean of the Graduate School and
Distance Education

# Acknowledgments

First of all, I would like to thank Dr. David Bailey for becoming my research adviser. I went to his office about two and a half years ago with a topic about biodiesel and even though the topic was not his research area, he accepted the position to be my research adviser. He has given me good advice and knowledge since the moment we started. I also like to thank the other professors in chemistry department and my committee members, Dr. Malonne Davies, Dr. Kim Simons, and Dr. Jorge Ballester for their time and helpful comments. I acknowledge R3 Energy LLC. and MidContinental Chemical Co. Inc. for providing their products as well as the Emporia State University Research and Grants Center for their financial support for this project.

Also, I am most grateful to my family, friends, and neighbors for their support. Most of all, I would like to express my gratitude to my encouraging and patient fiancé Mauricio and our Rottweiler Maverick D.C. who always be there for me and became my biggest supporters.

# Table of Contents

# List of Tables

Table Number Page

# List of Figures

# BACKGROUND

## History of Biodiesel

Oils and fats from biomass had been used as automobile fuels in the past. Rudolf Diesel who invented a diesel engine in 1894, tested his diesel engine on peanut oil at the 1900 World's Fair in Paris.[1] However, the direct use of vegetable oils had many issues such as high viscosity, low volatility, and incomplete combustion which leads to the formation of deposits causing the clogged injector.[2] The application of vegetable oil as fuels decreased as the rapid increase of supply for inexpensive and abundant petroleum. Petroleum has been the dominant fuel in our society for many decades. However, the concern toward environment and energy security drove an attraction toward alternative fuels.

The Clean Air Act Amendments (1990) and the Energy Policy Act (1992) ordered the use of alternative fuels in some trucks and buses in the United States.[1] The name of one of the alternative fuels produced from vegetable oils was introduced in the United States in 1992 as Biodiesel by the National Soy diesel Development Board.[3] Biodiesel is also known as FAME which stands for fatty acid methyl esters. The use of biodiesel in the United States increased significantly after the amendments to the Energy Policy Act were enacted into law in 1998.[1] Biodiesel is biodegradable fuel, which has lower emissions of pollutants such as carbon monoxide, particulates, hydrocarbons, soot, and sulfur oxide than petroleum or traditional diesel and also has capability to use petroleum diesel engines with little or no modifications.[4] Biodiesel is already commercially available in many countries such as the United States, Austria, the Czech Republic,

France, Germany, Italy, Malaysia, and Sweden.[1] These countries typically use biodiesel mixtures with petroleum like B20, which indicates mixture of 20% biodiesel in traditional diesel.

**Transesterification and Purification of Biodiesel**

One of the most common methods to synthesize biodiesel is called transesterification shown in Figure 1, which converts oils and fats to fatty esters using catalyst and alcohol.[5]

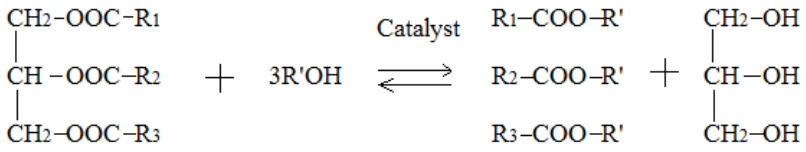


Figure 1. Transesterification reaction of oils and fats with alcohol and catalyst to produce esters and glycerol.

Since properties of biodiesel are directly affected by the structure of oils and fats, it is important to understand the compositions of raw materials. Oils and fats are primarily water-insoluble and consist of triglycerides. Triglycerides have structure of glycerol backbone with various fatty acids attached to it.[6] The properties of triglycerides can be determined by the lengths of fatty acid and numbers of double bond.[4a] In addition to the structure of raw materials, types of alcohol can influence the properties of biodiesel.[7] A previous study showed that the use of isopropanol gave better biodiesel properties than methanol, but due to the high cost of isopropanol, methanol or ethanol are often employed.[7] Base and acid catalysts are the two major catalysts applied to complete

transesterification. Base catalysts such as sodium hydroxide and potassium hydroxide remove a proton from alcohol to produce alkoxide and the protonated catalyst leads to nucleophilic attack of alkoxide to the carbonyl group of triglyceride.[5] However, producing biodiesel from oils which contain high free fatty acids with base catalyst can create soap, which reduces the amount of product thus acid catalysts like sulfuric acid are typically favored for those oils.[8]

Yield of transesterification is influenced by types of catalyst, amount of alcohol, reaction temperature and time, mixing intensity, free fatty acid contents, and water contents. Water consumes catalyst and forms stable emulsions which inhibit separation of glycerol from fatty esters, thus reducing yield of biodiesel.[6, 9] Even the use of refined natural vegetable oils can still contain small amount of water after purification.[4a] Therefore, elimination of water by preheating oils is important to achieve high yield. Also, water can be produced from reaction between catalyst and alcohol.[4a] Molecular sieves showed effectiveness lowering water productions and shifted the reaction toward the ester formation.[10] Freedman et al. suggested that alcohol to oil molar ratio of 6:1 with 1% sodium hydroxide gives the optimum condition for the reaction.[11] In addition, a previous study showed that less than 0.06% w/w and 0.5% w/w of water and free fatty acid content of beef tallow gave best results for transesterification using sodium hydroxide.[9b]

Byproducts and impurities also influence characteristics and performance of biodiesel and the engine life.[4a] Crude biodiesel contained many impurities from the

reaction such as free glycerol, soap, free fatty acids, excess alcohol, catalyst, water, and glycerol.[12] Therefore, purification steps are necessary to remove those impurities. A water wash is the most common method for a wet wash purification used in industries.[13] Glycerol and methanol are both water soluble so it is easy to remove these major impurities by the water wash.[12] On the other hand, synthetic magnesium silicate, silica gel, smectitic clay containing silica gel, and ion exchange resin are commonly used for a dry wash purification.[13-14]

**Physical Properties of Biodiesel**

The structural features of individual fatty esters determine the physical properties of biodiesel including ignition quality, heat of combustion, exhaust emissions, oxidative stability, cold flow, viscosity, density and lubricity. The quality specifications have to fulfill with the European standard specification (EN) 14214 or American Society for Testing and Materials (ASTM) D6751.[15] Thus, it is critical to identify the chemical structures of biodiesel in order to understand overall fuel properties. Compositions of biodiesel are generally analyzed by instrumentals such as gas chromatography-mass spectroscopy (GC/MS), Fourier transform infrared spectroscopy (FTIR), nuclear magnetic resonance spectroscopy (NMR), and high-performance liquid chromatography (HPLC).

Fuel is sprayed into compressed air and broken down into small droplets forming cone shape so viscosity is major factor to determine the atomization quality, size of droplets, and spray growth.[16] High viscosity fuel tends to have a lower spray cone angle

and larger droplet size which requires higher pumping power.[16] Also, high viscosity increases poor atomization performance, which leads to operational issues such as breakage of the fuel pumps and injectors.[17] On the other hand, low viscosity can cause lubrication issue.[18] According to the ASTM D6751, the kinematic viscosity of biodiesel have to meet the requirement of value between 1.9 to 6.0 centistokes (cSt) at 40ºC.[19] Longer fatty esters have higher viscosity than shorter fatty esters.[18] Moreover, Rodrigues and coworkers reported that one double bond increases viscosity due to stronger interactions between p electrons of double bonds than no double bond, which has only van der Waals interaction.[20] On the other hand, two or more double bonds have spatial geometry which weakens interactions between p orbitals and leads to a reduction of viscosity.[18] In addition, density is one of the physical properties that affects directly engine performance characteristics related to other quality measurements such as a heating value and a combustion quality.[17] Density increases as the number of double bonds increases and chain length shortens.[18] However, low density impurities such as methanol can reduce density.[18]

In addition to kinematic viscosity and density, cold flow characteristics are important parameters for biodiesel because of its poor cold weather properties.[4d] The temperature when biodiesel starts cloudy due to a formation of particles is called a cloud point (CP). The temperature when the fuel no longer flows is called a pour point (PP). As the temperature decreases below the CP, particles continue to grow and aggregate causing plugged fuel filters and pipes.[21] Common traditional diesel have -16ºC and -27ºC for the CP and the PP on the other hand, biodiesel produced from soybean oil typically

have 0ºC and -2ºC of the CP and the PP.[18] Molecular interactions have significant effect on crystallization. Saturated compounds crystallize faster than unsaturated compounds due to double bonds structures.[22] Double bonds provide the spatial geometry which prevents from packing at lower temperature. Biodiesel derived from beef tallow or palm oil contains high amount of saturated compounds have much higher CP than biodiesel derived from canola or linseed oil. It has been reported by Rodrigues *et al*. that double bonds located near the ends of carbon chain can pack more efficiently than double bonds found in middle of carbon chain.[18] Not only double bonds but also chain lengths affect properties in low temperature.[23] Other studies showed that branched carbon chains can crystallize slower than linear carbon chains which have larger van der Waals attractions.[24]

There are several approaches to improve the cold weather properties of biodiesel. The first method is blending biodiesel with traditional diesel.[25] Since traditional diesel is mainly consisted of hydrocarbon, mixture of biodiesel and petroleum diesel can reduce crystallization temperature. The second method is called winterization and this method removes components which have higher melting point by separation processes. However, this method is highly expensive in biodiesel production process.[26] In addition, removing saturated compounds results in decreasing the ignition quality and calorific value.[27] The third method is adding additives in biodiesel. Polymers and copolymers are commonly used as pour point depressants and wax dispersants.[28] In general, those additives have oil-soluble long chain alkyl group with polar structure moiety which can interfere the host material in molecular-level and prevent aggregation process of wax and particles due to

the polar moiety.[25-26, 29] Various analysis techniques for the CP have been reported such as visual observation, turbidimetry, light scattering, viscometry, thermo-optical analysis, neutron scattering, microcalorimetry, refractometry, near-infrared/fiber optic technique analysis and particle counting.[30] The common way to examine the CP is by ASTM D2500 which measures the CP visually however, frequent inspections are necessary.[31]

The temperature when biodiesel freezes below the PP is called a freezing point (FP). Sajith and coworkers showed that metal additives especially manganese has a great effect in the reduction of the FP.[32] Differential scanning calorimetry, thermomechanical analysis and dynamic mechanical analysis are useful to analyze the FP.[33] However, those methods require expensive instruments. On the other hand, the cooling curve method is easier, accurate, and cheaper to analyze. Typical cooling curve shown in Figure 2 illustrated freezing process for various situations.

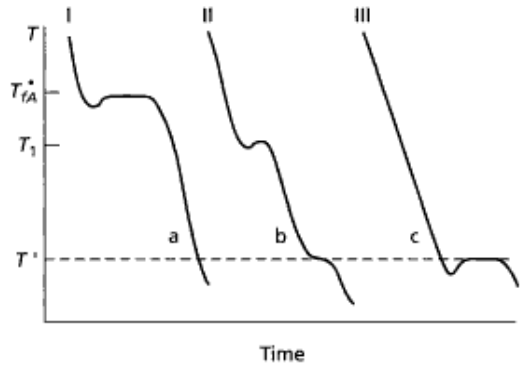


Figure 2. Typical cooling curves. I: pure solvent, II: mixture of solvent and solute, III: mixture of solvent and the eutectic composition.[34]

The temperature of a sample decreases gradually and goes into the super cooling phase and starts to solidify.[34] Then, a sudden increase in temperature to the FP is obtained by the faster release in its latent heat to the surroundings than the removing heat from the system.[33] During the solidification, the temperature stabilizes and the cooling curve levels off. After the crystallization is completed, the temperature decreases as cooling resumes. Figure 2 (I) graph shows a pure solvent cooling curve which have steady stabilization temperature. Two phase cooling curve can be seen in Figure 2 (II) which indicates that this solution is a mixture. Figure 2 (III) graph shows eutectic composition in mixture. The solute crystals form by releasing latent heat of crystallization causing slight increase in temperature.[33]

**Study Goals and Design**

In this study, two different biodiesel analyses were investigated. First, several desiccants including molecular sieves and calcium-based desiccants were chosen as the dry wash purification materials and compared especially removing volatile compounds from crude biodiesel. Calcium chloride and calcium sulfate, which are well known desiccants, were applied. In addition, 4A, 5A, 13X molecular sieves which are widely used for purification, separation, chemical sensors, optoelectronic devices, shape-selective catalysis, ion exchange, and desiccant due to their well defined various pore structures were employed.[35] The pore sizes of 4A, 5A, and 13X are 4, 5, and 10 angstroms respectively. Since both types of desiccants have a capacity to absorb chemicals, they have potentials to remove some of the volatile compounds from crude biodiesel. In addition, these desiccants can be reused after a reactivation.

Second, chemical and physical properties including the kinematic viscosity, the density, the CP, and the FP of canola oil, coconut oil, soybean oil, palm oil, and lard based biodiesel with Bio Flo, Wintron XC30, Wintron XC40, and Wintron Synergy additives were examined. While these properties were studied, new CP methodology was also developed. Since a particle formation is critical to analyze the CP, one way to determine the particle formation, light scattering, was applied. One of the common light scattering is called Rayleigh light scattering (RLS) and it is the scattering of light due to the elastic collisions of particles which are small compare to the wavelength of incident light.[36] The RLS is commonly used in biological analysis like study of proteins, structure of various types of complexes, and aggregation of dyes. However, determination of the CP by the RLS has never been investigated.

# EXPERIMENTAL

## Materials

Castor, canola, coconut, soybean, and palm oils were obtained from Jedwards International, Inc. (Quincy, MA). Lard (Armour Lard, Omaha, NE) and pure canola oil (The J.M. Smucker Company, Orrville, OH) was purchased from a local grocery store. Calcium chloride and calcium sulfate were purchased from Mallinckrodt and Drierite respectively. Three various types of additives: Wintron XC30, Wintron XC40, and Wintron Synergy were purchased from Biofuel Systems Group Limited (Lancashire, England). Bio Flo additive was supplied by MidContinental Chemical Co. Inc. (Olathe, KS). Factor Four Capillary Columns (30 m × 0.25 mm) was purchased from Varian Inc. (Palo Alto, CA). R3 biodiesel (R3) was supplied by R3 Energy LLC. (Cottonwood Falls, KS). The following chemicals were purchased from Fisher Scientific Co. (Pittsburgh, PA): methanol (HPLC Grade); potassium hydroxide (ACS certified, purity >86.9%wt); n-hexane (95% purity); 4A, 5A, 13X molecular sieves; triton X-100; concentrated nitric acid; n-pentanol; mineral oil; calcium hydroxide.

## Procedures

Biodiesel was synthesized by transesterification and impurities were removed by purifications. Cold soak filtration process and additives were employed for biodiesel to compare cold weather properties.

Transesterification of Biodiesel

Crisco Canola (Crisco CA-FAME), castor (CAS-FAME), canola (CA-FAME), coconut (CO-FAME), soybean (SO-FAME), palm oil (PA-FAME), and lard (LA-FAME) based biodiesel were synthesized in a 1000 mL Erlenmeyer flask with a magnetic stirrer rate of 600 rpm. Approximately 1000g of oils were preheated for 30 minutes above 100°C to eliminate excess moisture and in a separate flask, 1% (wt/wt) potassium hydroxide were mixed with methanol at a 6:1 methanol to oil molar ratio.[37] Mixture of catalyst and alcohol was added to the flask which contained oils and heated to 65°C for 120 minutes. After the reaction, the mixture was equilibrated to a room temperature and transferred to a 2000 mL separatory funnel followed by an overnight settling. A bottom layer, glycerol, was removed by a gravity separation.

Purification of Biodiesel

The crude FAMEs from Crisco pure canola oil were purified by calcium-based desiccants and molecular sieves to examine the removal of volatile byproducts. Wet wash purification by acid solution was used to compare the results. Detail procedures are listed in the analytical methods section. Other crude FAMEs were purified by the water washing after removing excess methanol by a rotary evaporation. Approximately 50 °C warm distilled water was used to wash crude FAMEs in the separatory funnel.[38] Excess water was removed by the rotary evaporation.

Cold Soak Filtration of Biodiesel

A standard method (ASTM D6751-09a) was modified for the cold soak filtration (CSF) to investigate differences in a cloud point (CP).[39] Approximately 20 mL of biodiesel was placed in a large glass test tube and set it in Thermo NESLAB RTE 10 digital One re-circulating thermostatic bath (Thermo Electron Company, Waltham, MA) at 1 °C above the cloud point for 8 hours. Then, the sample was slowly warmed up to a room temperature without adding additional heat. The sample was filtered through a vacuum filtration system with a single 0.45μm filter paper (0.45μm membrane MCE-47mm Non-sterile white, Fisher Scientific Co., Pittsburgh, PA) and separated into solid and liquid phase.

Preparation of Biodiesel with Additives

Wintron XC30 and XC40 additives which are pour point depressants, Wintron Synergy additive which is cold filter plugging point depressant, and Bio Flo additive which is cold flow improver were used as additives. The concentration for Wintron additives (XC30, XC40, and Synergy) was 2% (wt/wt) and the concentration of Bio Flo in the biodiesel was 0.5% (wt/wt).

**Analytical methods**

Purification process using desiccants and chemical and physical properties of biodiesel were studied.

Purification of Biodiesel by Desiccants

Removability of volatile byproducts was examined by various desiccants. Reusability and a saturation level of desiccants and calcium concentration were investigated.

*Determination of Volatile Byproducts Content in Biodiesel*

The volatile byproducts content was determined using a method AOCS Ca 2c-25.[40] Approximately 5% (wt/wt) of calcium chloride, calcium sulfate, 4A, 5A, or 13X molecular sieves were weighed and placed in 5 g of crude Crisco CA-FAME individually and let set for 30 minutes with occasional stirrings. A combination of calcium sulfate and 13X was set for 15 minutes each, total of 30 minutes setting. Then, the desiccants were removed by the vacuum filtration followed by oven dry at 101± 1$^{o}$C in a Fisher Isotemp Oven Senior Model (Fisher Scientific, Pittsburgh, PA). The sample was weighed after 1.5 hours to 2 hours then after that, it was weighed every 30 minutes until a constant weight was obtained. The volatile byproducts content in biodiesel was calculated by the amount of lost weight over the initial amount of sample. Crude Crisco CA-FAME was also washed with 5% (wt/wt) phosphoric acid solution in the separatory funnel.[41] Then, the volatile byproducts content of washed crude Crisco CA-FAME was determined and the results were compared with various desiccants.

*Determination of Reusability of Desiccants*

The excess FAMEs were removed from used desiccants and the desiccants were reactivated at 300$^{o}$C oven for 24 hours. The reusability of calcium chloride, calcium

sulfate, 4A, and 5A desiccants was calculated by the difference in the amount of desiccants after reactivation.

*Determination of Saturation Level of Desiccants*

The saturation of desiccants was determined by a glass column. Approximately 5 cm height of the glass column was packed with calcium sulfate and 13X individually and also combination of calcium sulfate and 13X. Crude Crisco CA-FAME was poured into the glass column and samples were collected every 15 seconds in a beaker. Then, the volatile byproduct content was analyzed by the same procedure which was explained in determination of volatile byproducts content in biodiesel section. The saturation graph was plotted with the amount of volatile byproducts present in biodiesel as the function of time.

*Determination of Calcium Content in Biodiesel*

The calcium concentration of biodiesel was analyzed by AAnalyst100 atomic absorption spectrometer (Perkin-Elmer, Norwalk, CT). Standard solutions were prepared by mixing 57.6% (wt/wt) n-pentanol as co-surfactant, 20% (wt/wt) mineral oil, 14.4% (wt/wt) triton X-100, and 8% (wt/wt) water.[42] In the water content, 1000 ppm calcium hydroxide was added to achieve the final calcium concentration of 1, 2, 5, 8, and 10 ppm. Biodiesel samples were prepared the same procedure except changing mineral oil to biodiesel. A calibration curve was obtained using the data of standard solutions and the calcium concentrations of the samples were calculated.

Chemical Properties of Biodiesel Analysis

Chemical properties of biodiesel were analyzed by FTIR, NMR, and GC/MS.

*Fourier Transform Infrared Spectroscopy Analysis*

Fourier transform infrared spectroscopy (FTIR) spectra of transmittance were obtained using Spectrum One FTIR Spectrometer (Perkin-Elmer, Norwalk, CT) with diamond ATR. Scanning range of 650-4000 $cm^{-1}$, scan number of four, and resolution of 4 $cm^{-1}$ were employed for this analysis.

*Magnetic Resonance Spectroscopy Analysis*

$^{1}H$ magnetic resonance spectroscopy ($^{1}H$-NMR) spectra were recorded using Eft-90 NMR spectrometer (Anasazi Instruments, Indianapolis, IN). 500 µL of sample was diluted in 500 µL carbon tetrachloride. One scan was collected for this experiment.

*Gas Chromatography Mass Spectroscopy Analysis*

Gas chromatography-mass spectroscopy (GC/MS) spectra were recorded on Varian Saturn 2100T with 30 m × 0.25 mm × 0.25 um Rtx-Wax column (Restek, Bellefonte, PA). Split ratio of 1:10, injection temperature of 220°C, flow rate of 1 mL/min were applied for GC instrumental setting. Initial oven temperature was 160°C followed by increase of temperature up to 200°C with 20 °C/min and increase up to 230°C with 5 °C/min and hold for 6 minutes.[43] Detection delay for MS of 1.6 minutes was employed. The ratio of sample to solvent, hexane, were 1:400.

Physical Properties of Biodiesel

Kinematic viscosity, density, cloud point, and freezing point of biodiesel were investigated.

*Determination of Kinematic Viscosity*

The kinematic viscosity was determined with a size 100 Cannon-Fenske Routine viscometer (Cannon Instrument Co., Boalsburg, Pa) at 40°C followed by ASTM D445-09.[44] The temperature of a water bath was set at 40°C and calibrated. 10 mL of sample was placed into the viscometer and allowed the viscometer and sample to equilibrate to the water bath for 30 minutes. Sample liquid was sucked above the top mark using a vacuum hose and time required to travel from the top mark to the bottom mark was timed. All experiments were run in quadruplicate and the kinematic viscosity was calculated by the following equation (1)

$$v = C \times t \quad (1)$$

Where $v$ is the kinematic viscosity (centistokes, cSt), $C$ is the viscometer constant (cSt/s), and $t$ is the measured flow times (s). Then, an average kinematic viscosity and a standard deviation were reported.

*Determination of Density*

The density was calculated by the following equation (2).

$$\rho = \frac{m}{V} \quad (2)$$

Where $\rho$ is the density (g/mL), $m$ is the mass (g), and $V$ is the volume (mL). Mass and volume were measured using a 10 mL volumetric flask at the 25°C water bath.

Equilibrium time of 20 minutes was applied. All experiments were run in triplicate and an average density and a standard deviation were reported.

*Determination of Cloud Point*

Cloud point was studied by spectrofluorometer, visual observation, and ultraviolet-visible spectrophotometer.

SPECTROFLUOROMETRIC CLOUD POINT ANALYSIS METHOD

The fluorometer cloud point ($CP_F$) was determined using Horiba JobinYvon FluoroMax-4 Spectrofluorometer (HORIBA JobinYvon Inc., Edison, NJ) by measuring RLS. Approximately 2 mL of sample was placed in a 10 mm silica quartz cuvette. A width of excitation and emission slits was set at 1.0 nm. An excitation wavelength of 400 nm was used to probe the sample and a scattering of the excitation wavelength was measured from 200 to 600 nm at various temperatures from 25°C to -15°C with a 20 minutes equilibration time for every degree decrement. Changing in the light scattering was obtained by plotting temperature versus S1/R1 (signal over references). Then, a minimum distinguishable analytical signal (MDAS) was calculated according to the equation below.[45]

$$S_m = \overline{S_{bl}} + k s_{bl} \quad (3)$$

Where $S_m$ is the MDAS, $\overline{S_{bl}}$ is baseline, which is average blank signal obtaining at much higher temperature than the $CP_F$ of the sample, and an instrument noise was calculated as $k$ which is constant multiplied by $s_{bl}$, which is standard deviation of blank signal. Typically, $k = 3$ is applied in order to obtain 99.86% confidence level.[46] However, $k = 5$

was used in this experiment to achieve higher confidence level. The temperature at which the scattering signal was significantly higher than the sum of the baseline and the instrument noise was recorded as the $CP_F$. In addition, various equilibrium times from 1 to 20 minutes for both 10 mm and 3 mm cuvettes were employed to compare the minimum equilibrium time to determine the $CP_F$.

### Modified Visual Cloud Point Analysis Method

The visual cloud point ($CP_V$) method ASTM D2500 was modified to analyze the $CP_V$ of each sample. The sample was placed in the 10 mm cuvette. The cooling system was controlled by Horiba JobinYvon FluoroMax-4 Spectrofluorometer (HORIBA JobinYvon Inc., Edison, NJ). Temperature was adjusted from 298 to 258 K with the 20 minutes equilibration time for each temperature. The sample was checked for cloudiness each temperature and the temperature when the sample showed cloudy appearance was recorded as the $CP_V$.

### Ultraviolet-Visible Spectroscopic Cloud Point Analysis Method

The UV-vis cloud point ($CP_U$) was determined by Cary 50 Bio UV-Visible Spectrophotometer (Varian Inc., Palo Alto, CA, USA). The re-circulating thermostatic bath was used for control the temperatures. Stephen and coworkers showed that biodiesel absorbed light below 400 nm and particles scattered short wavelength light more effectively than long wavelength light.[47] Therefore, a transmittance at 540 nm was applied. The transmittance was plotted as a function of temperature and the temperature which has a maximum derivative was reported as the $CP_U$.

*Determination of Freezing Point*

Freezing point of biodiesel was analyzed and freezing point depression using hydrocarbon solutes was examined.

### Freezing Point Analysis of Biodiesel

Approximately 2 mL of sample was transferred into a small test tube and held with a clamp. A thermocouple temperature probe TC101A (MadgeTech, Contoocook, NH) was immersed into the sample solution without touching side of the test tube. The accuracy of the temperature probe was ± 0.5°C. The apparatus was placed into either -30°C Kelvinator freezer (Kelvinator, Charlotte, NC) or -80°C Fisher Isotemp freezer (Fisher Scientific, Pittsburgh, PA). Temperatures were recorded every second for 30 minutes. The cooling curve was obtained by plotting temperature versus time. The freezing point (FP) was identified at the temperature where the slowest cooling rate starts from the cooling curve.

### Freezing Point Depression of Biodiesel

Samples were prepared by mixing 3 mL CA-FAME as solvent with seven different types of solutes at various concentrations from 0 to 10 M. The solutes used in the FP depression experiment were heptane (C7), octane (C8), decane (C10), dodecane (C12), tetradecane (C14), hexadecane (C16), and octadecane (C18). Then, the FP was analyzed by applying the method described above. The relationship between the FP and various solutes at different concentrations were examined.

# RESULTS/DISCUSSION

**Volatile Byproducts Content in Biodiesel and Reusability and Saturation of Desiccants**

Figure 3 shows the results, which were run in triplicate, of the amount of volatile byproducts present in biodiesel produced from Crisco canola oil (Crisco CA-FAME) after with treatment and without any treatments (NT). The NT has a higher amount of volatile byproducts and the calcium-based desiccants were almost comparable to the acid wash. Among the molecular sieves, the adsorption of the volatile byproducts by 13X was higher than 4A and 5A. Overall, the calcium-based desiccants had better capability absorbing the volatile byproducts than the molecular sieves.

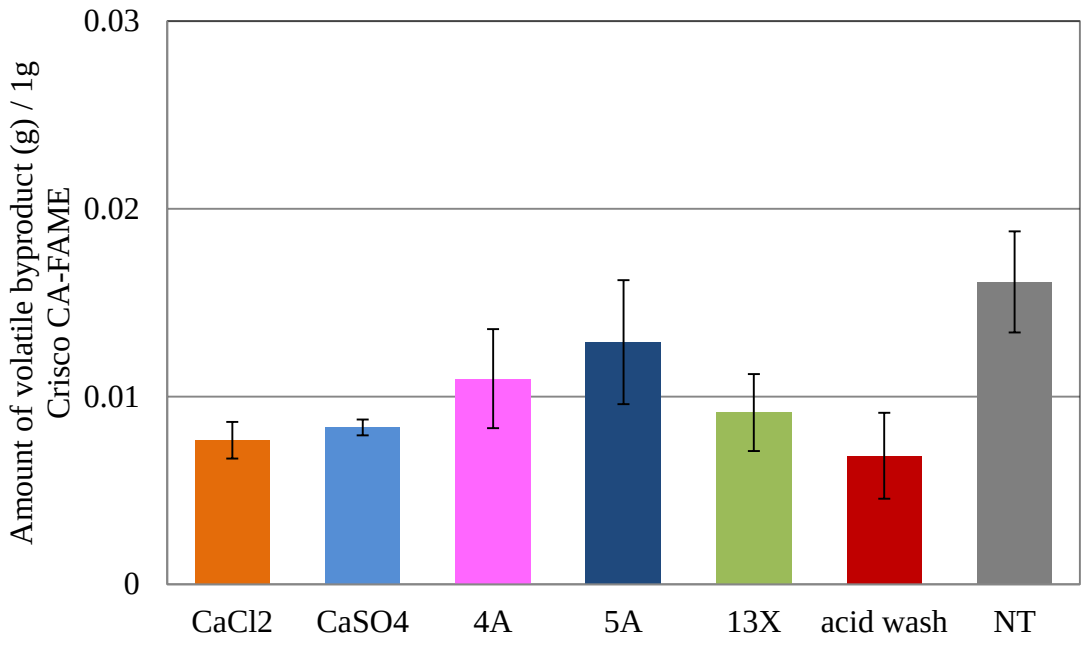


Figure 3. Comparison of average volatile byproducts content in Crisco CA-FAME which was removed by Ca based desiccants, molecular sieves, and acid wash and Crisco CA-FAME without any treatments (NT).

Table I shows very low recovery yield for calcium chloride losing about 30% of its weight after the reactivation process. A loss of calcium chloride might happen during the vacuum filtration since calcium chloride used in this study was fine powders. Also, Table II indicates that calcium dissolved in biodiesel because the calcium concentration of Crisco CA-FAME treated with calcium sulfate was much higher than that of Crisco CA-FAME without any treatments. The calcium concentration of Crisco CA-FAME treated with calcium sulfate was more than the limitation of calcium and magnesium combination value of 5 ppm listed in ASTM D6751.[48] Therefore, even though calcium sulfate was the most suitable reusable desiccants among various drying agents, biodiesel treated with calcium sulfate was inapplicable.

Table I Comparison of recovery yield of calcium chloride, calcium sulfate, 4A, and 5A molecular sieves after reactivation

| | Recovery yield (%) |
|---|---|
| $CaSO_4$ | 98.1 |
| $CaCl_2$ | 69.4 |
| 4A | 82.0 |
| 5A | 88.1 |

Table II Comparison of calcium concentration for crude Crisco CA-FAME with treatments of calcium sulfate and 13X molecular sieves and without any treatment

| | NT | $CaSO_4$ | 13X |
|---|---|---|---|
| Ca conc. (ppm) | 0.1 | 23.1 | BDL |

Then, the combination of calcium sulfate and 13X was investigated for the removability of excess calcium from biodiesel treated with the calcium-based desiccants by the molecular sieves. The experiments were run in triplicate and average volatile byproduct content was shown in Figure 4. Since this Crisco CA-FAME was synthesized in different batches, slight differences in the amount of the volatile byproducts between Figure 3 and Figure 4 were observed. However, calcium sulfate had again higher capacity to absorb the volatile byproducts than 13X. Crisco CA-FAME treated with the combination of calcium sulfate and 13X gave the lowest amount of the volatile byproducts which indicated the combination was more effective than applying individual desiccant.

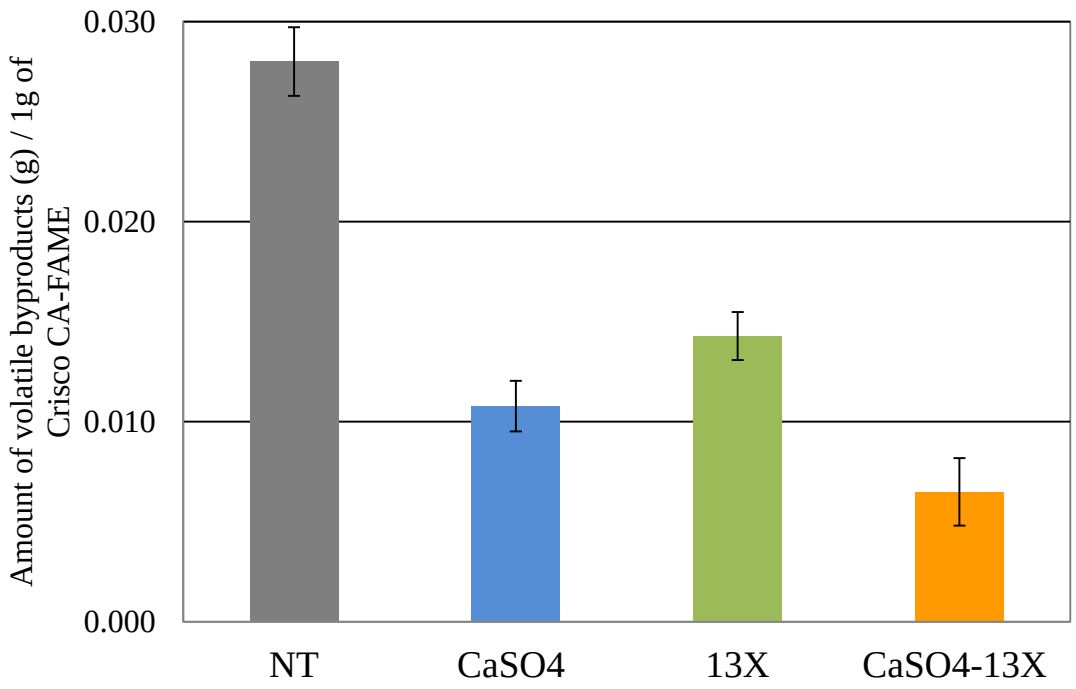


Figure 4. Comparison of average volatile byproducts content in Crisco CA-FAME which was removed by $CaSO_4$, 13X, and combination of $CaSO_4$-13X and Crisco CA-FAME without any treatments.

The change in values for the calcium concentrations between Table II and III was observed. This might be due to the size of calcium sulfate crystals. Calcium sulfate used in Table II might be smaller crystals than that used in Table III. Slight changes in standard solutions preparation might also contribute to this change. However, the calcium concentration was successfully reduced from 5.7 to 2.3 ppm using the combination of the calcium-based desiccants and the molecular sieves.

Table III Calcium concentration in crude Crisco CA-FAME treated with $CaSO_4$, 13X, and combination of $CaSO_4$-13X

| | NT | $CaSO_4$ | 13X | $CaSO_4$-13X |
|---|---|---|---|---|
| Ca conc. (ppm) | 1.0 | 5.7 | 0.8 | 2.3 |

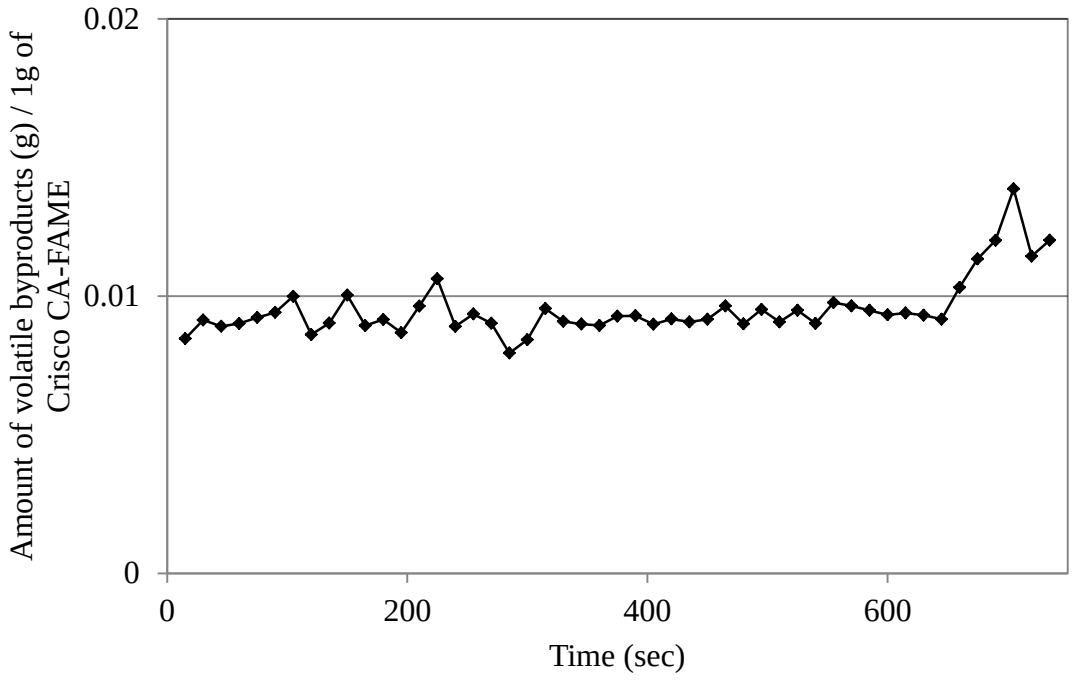


Figure 5. Saturation analysis of $CaSO_4$ using glass column.

The saturation analysis for calcium sulfate, 13X, and the combination of calcium sulfate and 13X were plotted in Figure 5, 6, and 7. Although the absorption capability using calcium sulfate was higher than 13X for the 30 minutes setting method, this saturation analysis shows that calcium sulfate and 13X individually had similar amount of the volatile byproduct contents in Crisco CA-FAME. The combination also shows higher absorption using the 30 minutes setting method compared with the glass column method. In addition, two distinguish level phases were observed for the combination of desiccants shown in Figure 7. This may indicate that the one of two desiccants reached its maximum saturation faster than the other but further examinations will be necessary to prove the theory.

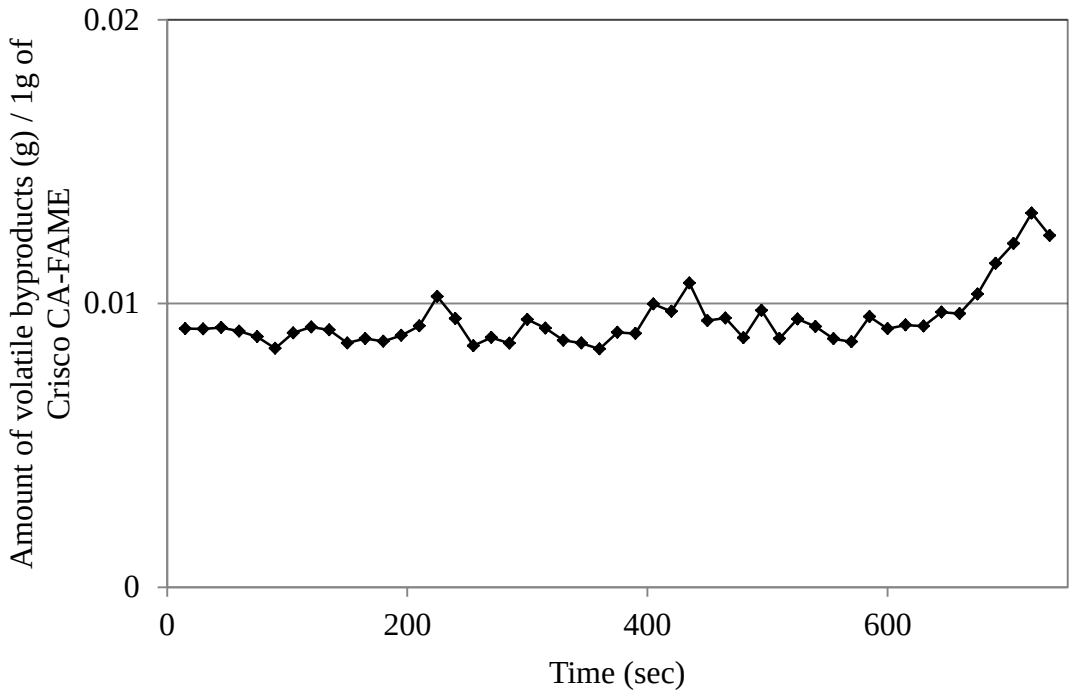


Figure 6. Saturation of 13X using glass column.

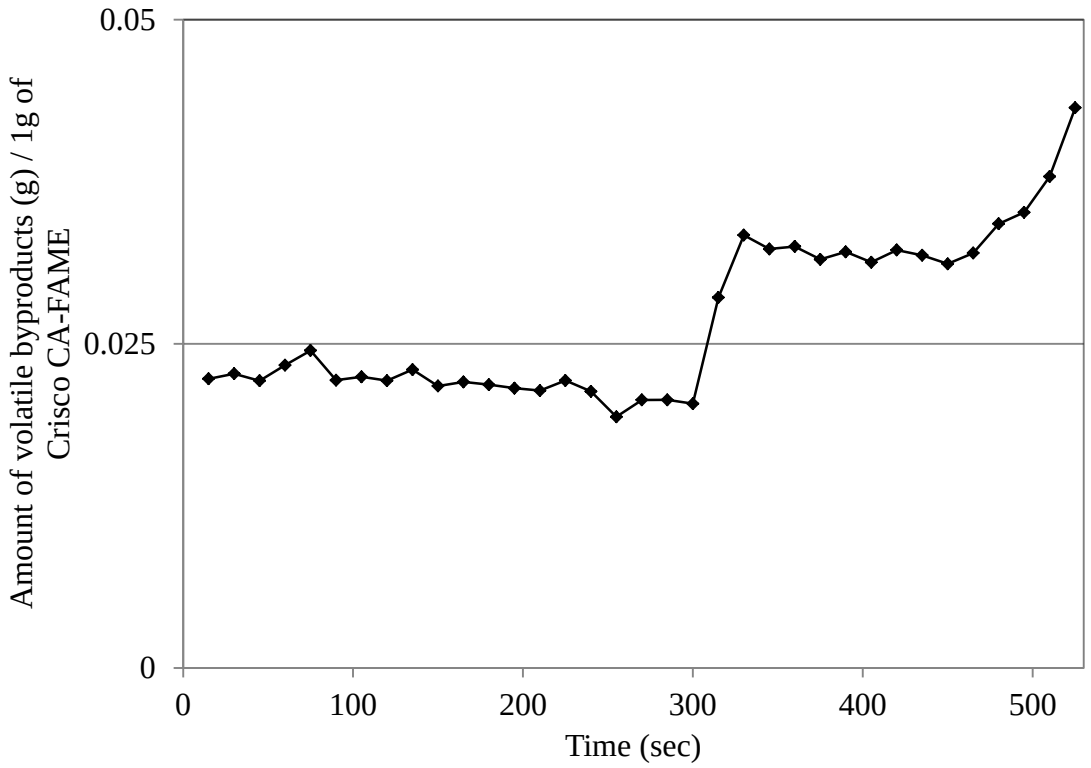


Figure 7. Saturation of combination of $CaSO_4$-13X using glass column.

**Chemical Compositions Analysis of Biodiesel**

Biodiesel produced from canola oil, coconut oil, soybean oil, palm oil, and lard (CA-FAME, CO-FAME, SO-FAME, PA-FAME, and LA-FAME) were successfully synthesized through transesterification. All FAMEs have similar FTIR peaks shown in Figure 8. Two peaks around 2950 and 3000 $cm^{-1}$ were C-H vibrations. Also, wave number of 1750 $cm^{-1}$ indicates C=O vibration of esters. According to Figure 9, the strong extra signal appeared in CA-FAME proton NMR spectrum which indicated methyl ester formations compared with the spectrum of canola oil. This extra peak was also observed in CO-FAME, SO-FAME, PA-FAME, and LA-FAME proton NMR spectra.

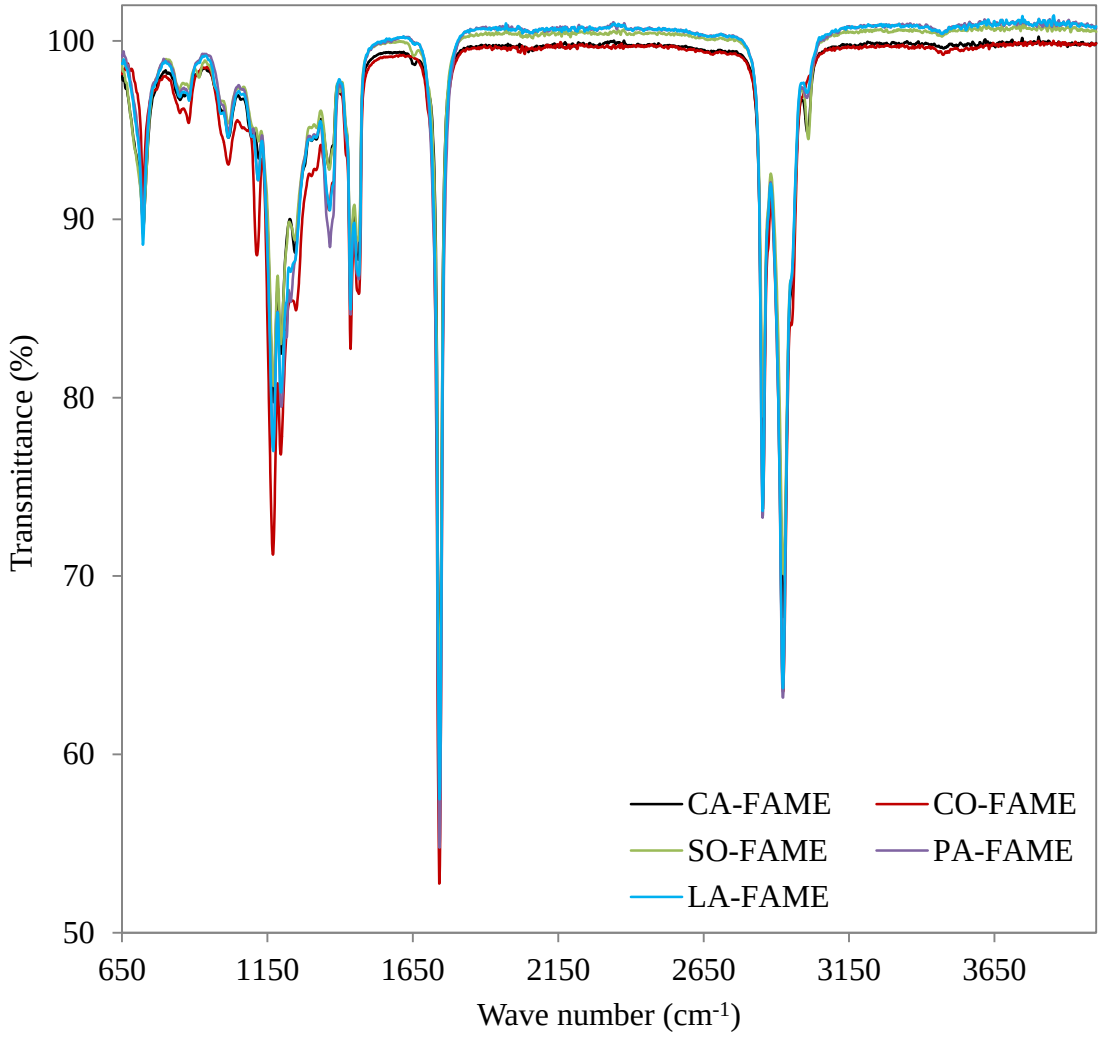


Figure 8. FTIR spectra from 650 to 4000 nm for CA-FAME, CO-FAME, SO-FAME, PA-FAME and LA-FAME.

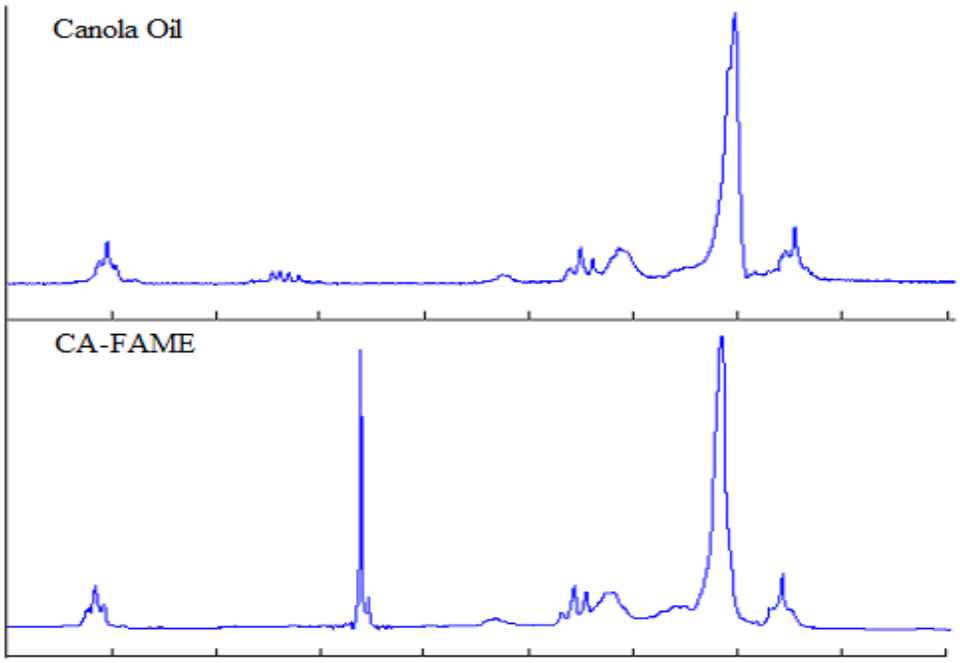


Figure 9. Comparison of $^{1}H$ NMR spectra of canola oil and CA-FAME.

However, biodiesel from castor oil could not be obtained due to an inability to separate glycerol from the product after transesterification. FTIR data in Figure 10 shows that an unseparated phase was a mixture of FAME and glycerol. Overlapped spectra of R3 and the unseparated phase at wave number of 1750 $cm^{-1}$ indicated the ester formation. However, the unseparated phase shows partial glycerol at 1000 $cm^{-1}$ and 3300 $cm^{-1}$. This may be due to a solubility of castor oil and its derivatives in alcohol.[49] They are completely soluble in alcohol thus; the complete transesterification reaction might not be achieved due to the lack of alcohol.

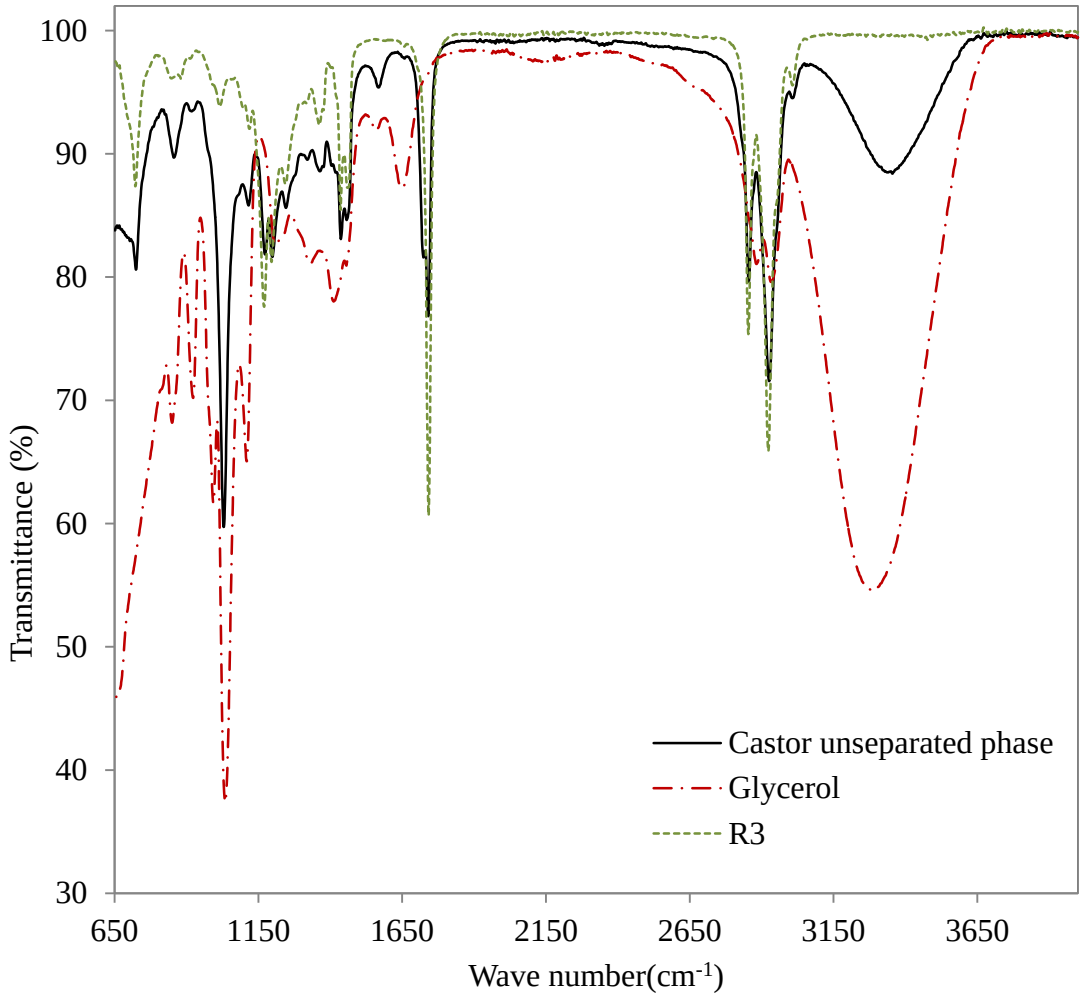


Figure 10. FTIR results from 650 to 4000 nm for unseparated phase from castor oil transesterification, glycerol, and R3.

Table IV Biodiesel profiles (area %) for various feedstock based biodiesel

| | CA-FAME | CO-FAME | SO-FAME | PA-FAME | LA-FAME |
|---|---|---|---|---|---|
| Caprylic (C8:0) | - | 6.3 | - | - | - |
| Capric (C10:0) | - | 6.3 | - | - | - |
| Lauric (C12:0) | - | 43.6 | - | - | 0.2 |
| Myristic (C14:0) | 0.1 | 21.5 | 0.1 | 1.4 | 2.4 |
| Pentadecylic (C15:0) | - | - | - | - | 0.1 |
| Palmitic (C16:0) | 6.5 | 11.5 | 12.2 | 39.1 | 25.6 |
| Palmitoleic (C16:1) | 0.3 | - | 0.2 | 0.2 | 2.7 |
| Margaric (C17:0) | 0.2 | - | 0.2 | 0.2 | 0.6 |
| Margaroleic (C17:1) | 0.3 | - | - | - | 0.4 |
| Stearic (C18:0) | 2.3 | 3.4 | 5.6 | 5.6 | 17.6 |
| Oleic (C18:1) | 63.6 | 6.3 | 24.2 | 41.2 | 33.6 |
| Linoleic (C18:2) | 17.3 | 0.8 | 45.5 | 10.4 | 12.4 |
| Linolenic (C18:3) | 6.2 | - | 6.8 | 0.2 | 0.2 |
| Arachidic (C20:0) | 0.4 | - | 0.4 | 0.5 | 0.3 |
| Eicosanoic (C20:1) | 0.8 | - | 0.2 | 0.2 | 0.5 |
| Eicosadienoic (C20:2) | - | - | - | - | 0.4 |
| Behenic (C22:0) | - | - | 0.2 | - | - |

Biodiesel profiles shows that CA-FAME and SO-FAME have a similarity in chemical compositions containing high amount unsaturation according to Table IV. Also, PA-FAME and LA-FAME had significantly higher amount of C16:0. The composition differences between SO-FAME and PA-FAME were observed the same way in a literature.[50] CO-FAME had a higher amount of shorter carbon chain fatty esters which can be predicted by the high amount of C12:0 and C14:0 fatty acid compositions in coconut oil.[3] After the cold soak filtration (CSF), PA-FAME formed insoluble particles which stayed in particles when the sample warmed up to the room temperature but solids phases from CA-FAME, CO-FAME, SO-FAME, and LA-FAME returned to liquid at the room temperature.

In addition, additives did not change much in chemical structures of biodiesel. Bio Flo additive is consisted of 45 to 65% light aromatic solvent naphtha, 30% 1,2,4-trimethylbenzene, 3% 1,3,5-trimethylbenzene, 3% xylene, 3% isopropylbenzene, and 1% naphthalene. Bio Flo additive chemical compositions can be seen in Figure 11. The GC spectrum of CA-FAME with Bio Flo shows 1,2,4-trimethylbenzene at 1.7 minutes according to Figure 12. Similar spectra were obtained for CA-FAME XC30 (Figure 13) and CA-FAME XC40 (Figure 14). Since XC30 and XC40 are both styrene copolymer esters in toluene, some of compounds in additives might create broad peaks at around 2 minutes might be due to the additives but no clear results were obtained. No chemical structure changes were observed for CA-FAME with Synergy additive. CO-FAME, SO-FAME, PA-FAME, and LA-FAME shows broad peaks with XC30, and XC40 additives and 1,2,4-trimethylbenzene peak for Bio Flo additive.

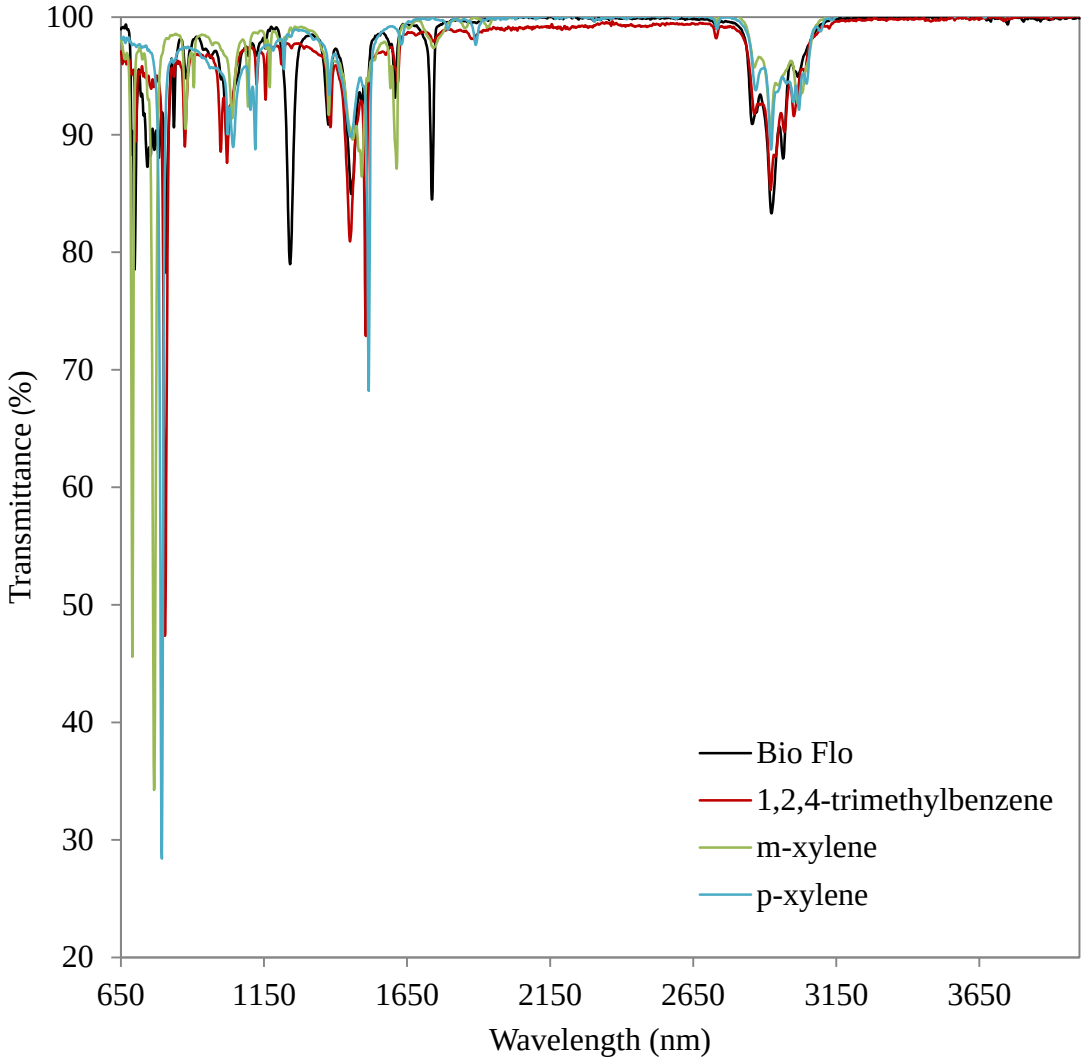


Figure 11. FTIR spectra from 650 to 4000 nm for additive Bio Flo and some of its compositions.

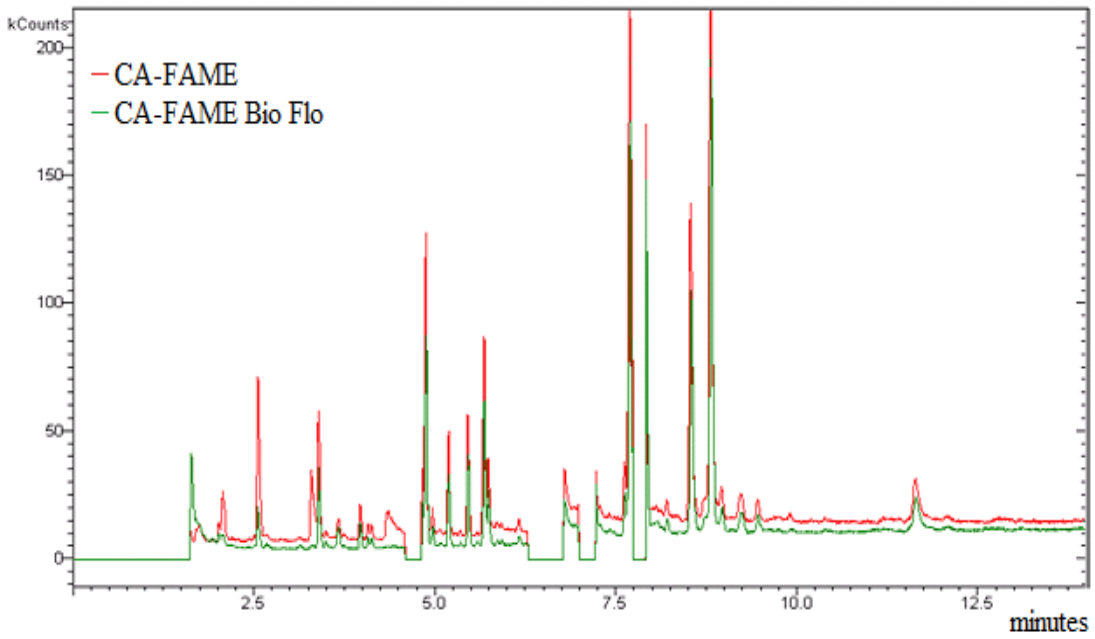


Figure 12. GC spectra of CA-FAME and CA-FAME with Bio Flo additive.

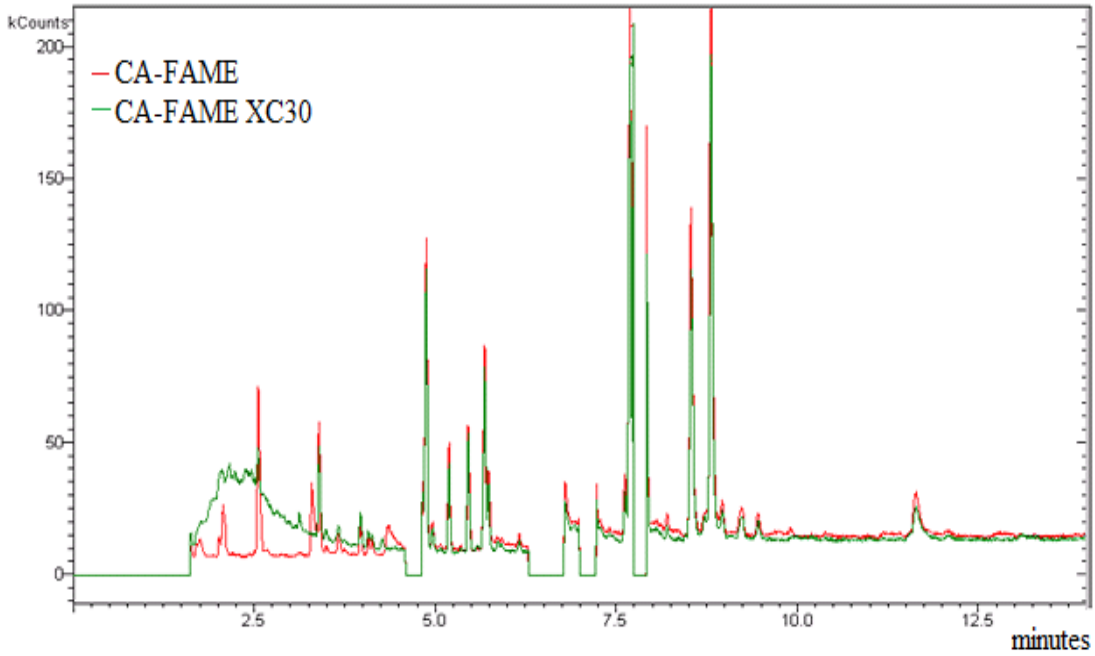


Figure 13. GC spectra of CA-FAME and CA-FAME with XC30 additive.

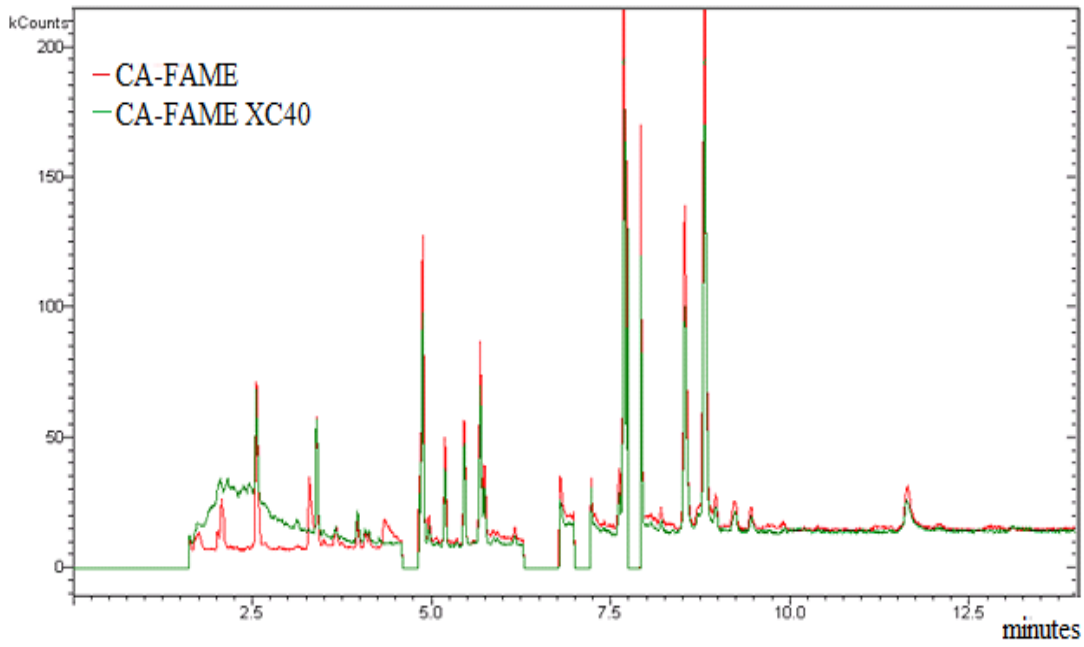


Figure 14. GC spectra of CA-FAME and CA-FAME with XC40 additives.

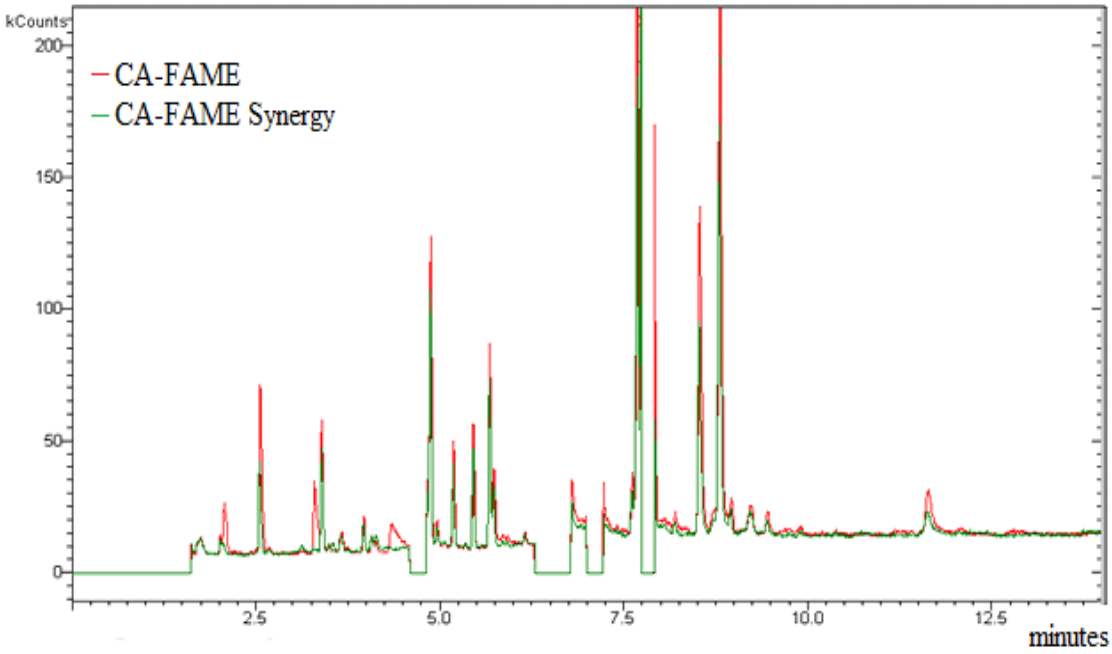


Figure 15. GC spectra of CA-FAME and CA-FAME with Synergy additive.

**Physical Properties of Biodiesel**

The viscosity experiments were run in quadruplicate and Figure 16 illustrates that adding viscous copolymer additives, XC30 and XC40, led to higher viscosity than the FAMEs without additive. The viscosity requirement of 6.0 centistokes (cSt) could not be achieved by CA-FAME, SO-FAME, PA-FAME, and LA-FAME with XC30 and XC40 additives therefore those additives were not applicable with that concentration. Since Synergy is mineral oil based additive, the viscosity increased slightly. The viscosity order of XC30 > XC40 > Synergy > Bio Flo was obtained. Shorter fatty asters of CO-FAME had the lowest viscosity which followed the general trend for viscosity.

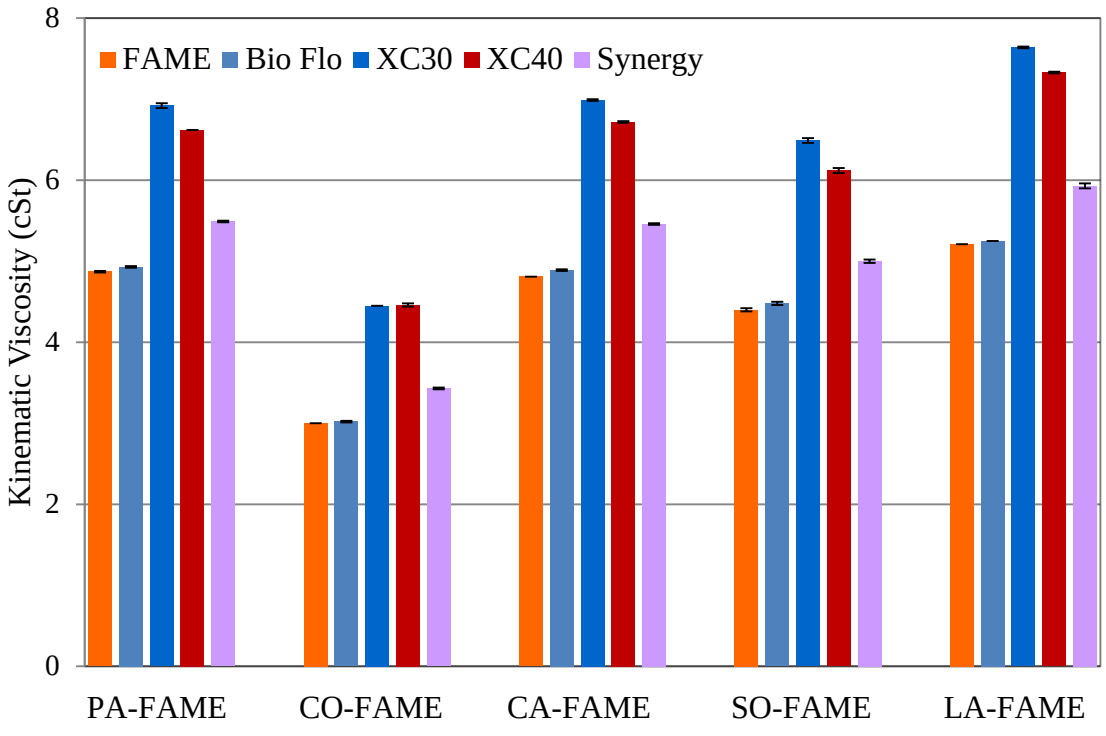


Figure 16. Summary of average kinematic viscosity (cSt) at 40ºC of various biodiesels and those with additives.

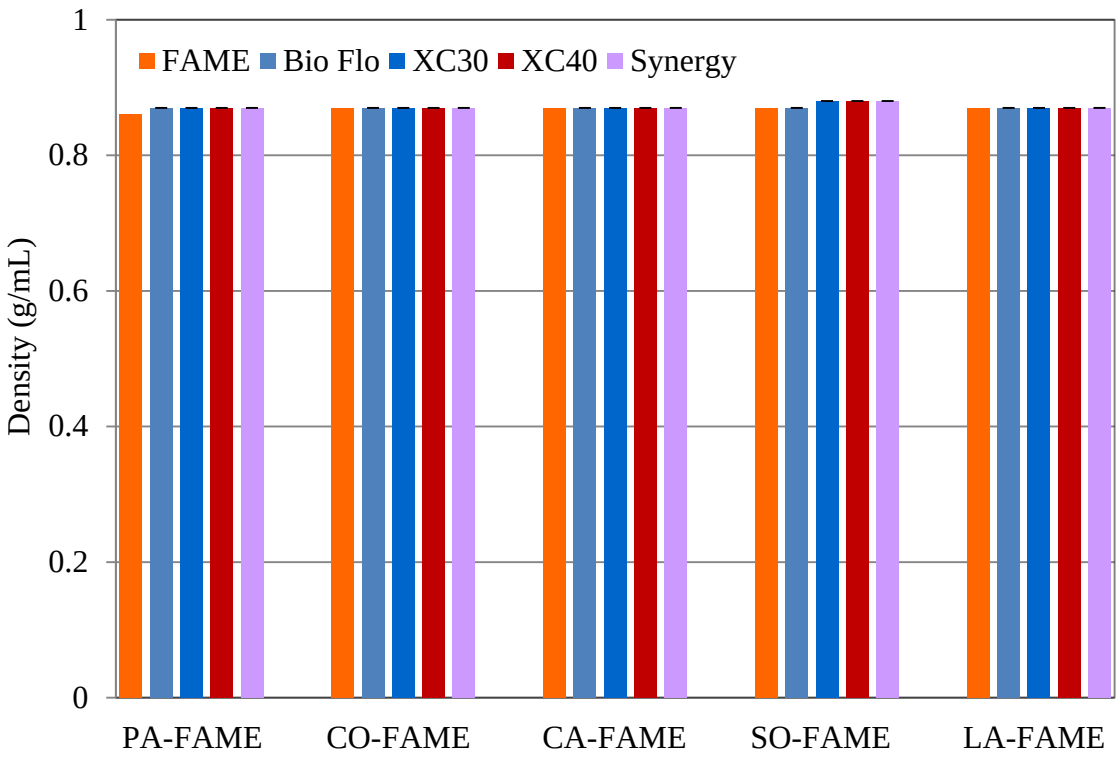


Figure 17. Summary of average density (g/mL) at 25ºC of various biodiesels and those with additives.

The density measurement done in triplicate shown in Figure 17 illustrates that CO-FAME and PA-FAME had lower density than CA-FAME, SO-FAME, and LA-FAME. Some of additives increased the density slightly.

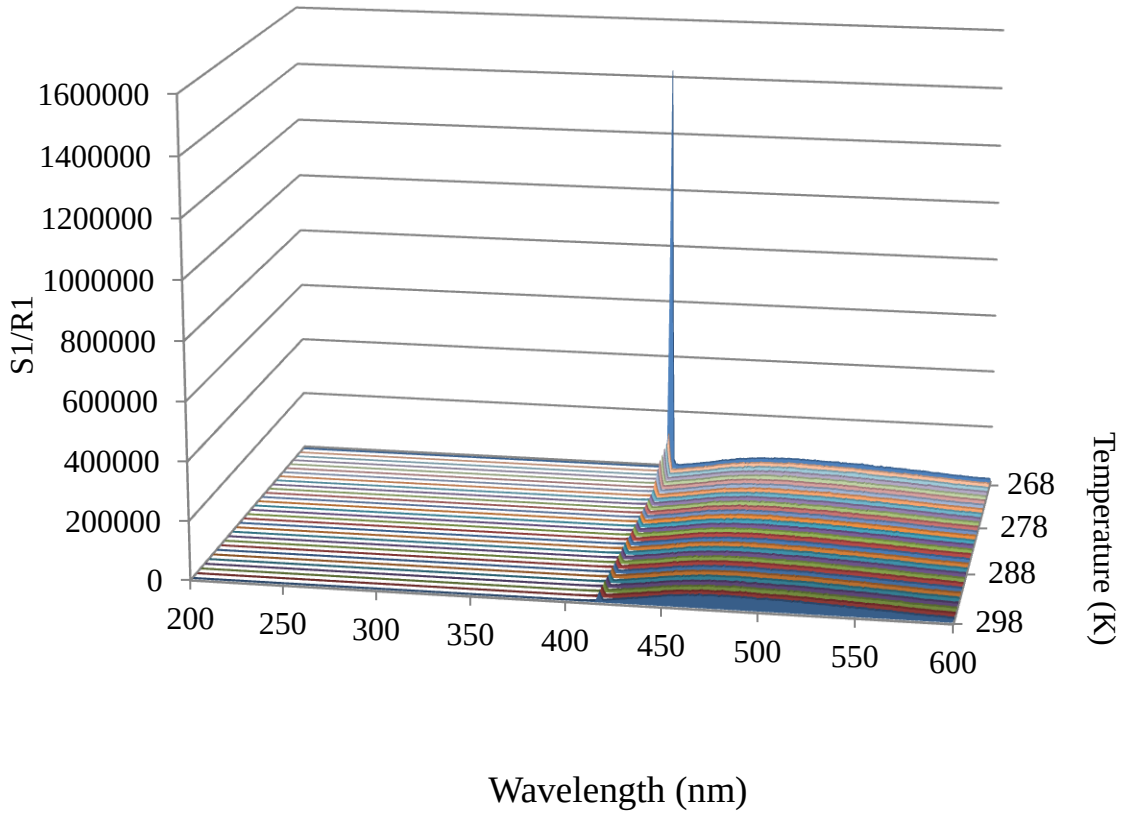


Figure 18. Three dimensional spectrofluorometer graph of CA-FAME with excitation wavelength of 400 nm.

Figure 18 shows a three dimensional graph of the Rayleigh light scattering (RLS) for CA-FAME. At around 415 nm, large increase in the intensity of the RLS as the temperature decreased was observed. Typically the excitation wavelength and scattering wavelength for RLS are the same but the shift in scattering wavelength was seen according to Figure 19.

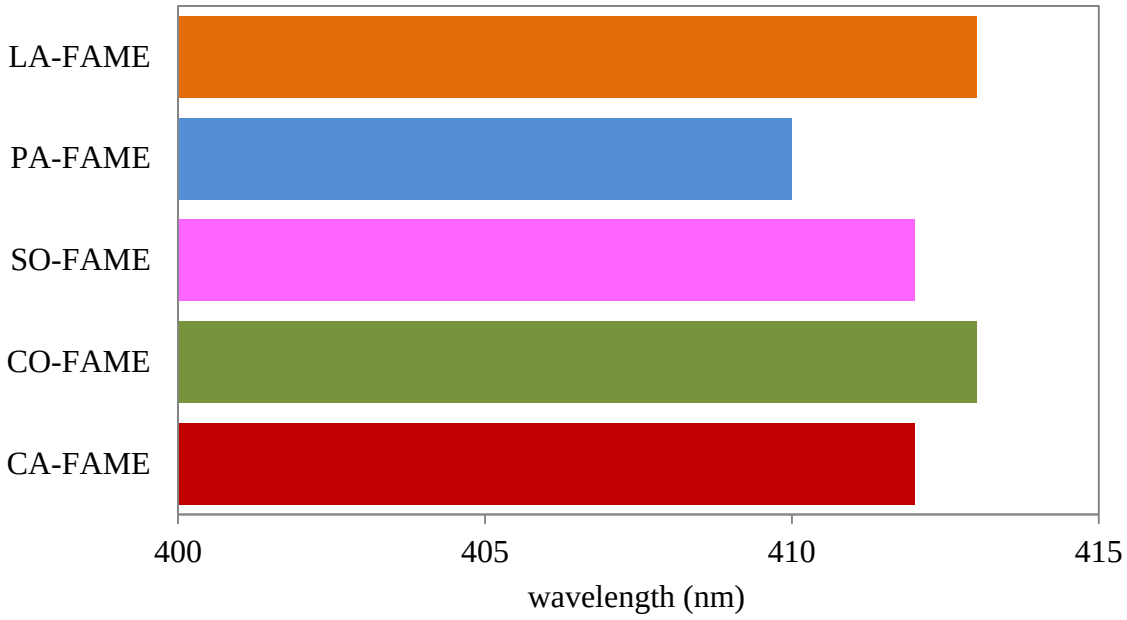


Figure 19. Average scattering peak for CA-FAME, CO-FAME, SO-FAME, PA-FAME, and LA-FAME compared with excitation wavelength of 400 nm.

This phenomenon is typically observed using resonance RLS.[51] Resonance RLS is produced when the wavelength of RLS is located at or close to molecular absorption band.[52] According to the study by Zhu and coworkers, as a dielectric constant of surrounding media increases, the scattering peak red-shifts.[53] Since the dielectric constant can be expressed using a refractive index in a following equation: $\varepsilon_r(\lambda) = n^2(\lambda) + k^2(\lambda)$ where $\varepsilon_r$ is relative dielectric constant, $n$ is real part of refractive index, $k$ is imaginary

refractive index, and λ is wavelength of incident light, the peak shift should be observed by the change of the refractive index.[54] Generally the refractive index of biodiesel gets larger as the lengths of carbon chain and levels of unsaturation increase.[55] Thus, biodiesel which contains longer carbon chains with high level of unsaturation such as CA-FAME, SO-FAME, and LA-FAME is predicted to have longer scattering wavelength than CO-FAME and PA-FAME. Figure 19 shows the larger shift for CA-FAME, SO-FAME, and LA-FAME and the smaller shift for PA-FAME which followed the general trend for the refractive index and the peak shift. However, CO-FAME shifted longer than CA-FAME and SO-FAME. This might be explained by the presence of impurities in CO-FAME such as glycerol. Glycerol has higher refractive index than typical biodiesel and could shifts the peak even further.[56]

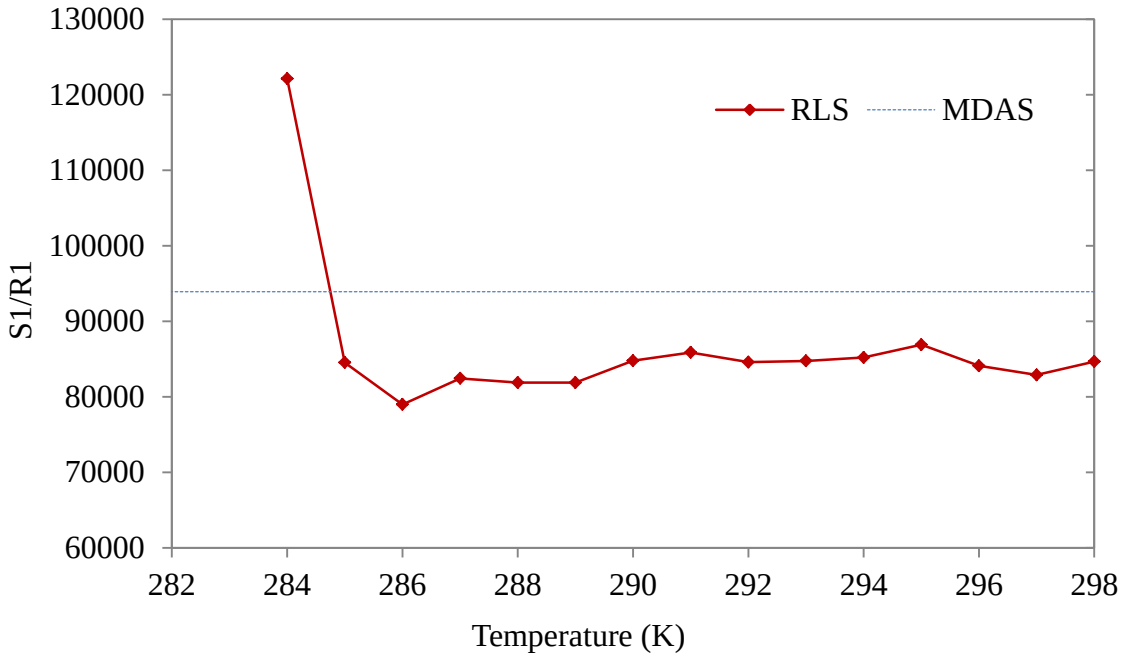


Figure 20. Plot of CO-FAME for fluorometer cloud point determination using Rayleigh light scattering (RLS) calculated by minimum distinguish analytical signal (MDAS).

To determine the fluorometer cloud point ($CP_F$), the emission of the RLS intensity was plotted as the function of time as shown in Figure 20. The graph illustrates CO-FAME sample using the fluorometer method and the minimum distinguish analytical signal (MDAS) was calculated above 286 K. From the graph, the temperature of 284K was significantly higher than the MDAS which indicated the presence of particles. Therefore, the 284 K was concluded as the $CP_F$ for CO-FAME. The UV-vis cloud point ($CP_U$) determination of CO-FAME can be seen in Figure 21. The sudden decrease in transmittance indicates the start of particle formation. The highest derivative of CO-FAME was obtained at 283 K thus, 283 K was recorded as the $CP_U$.

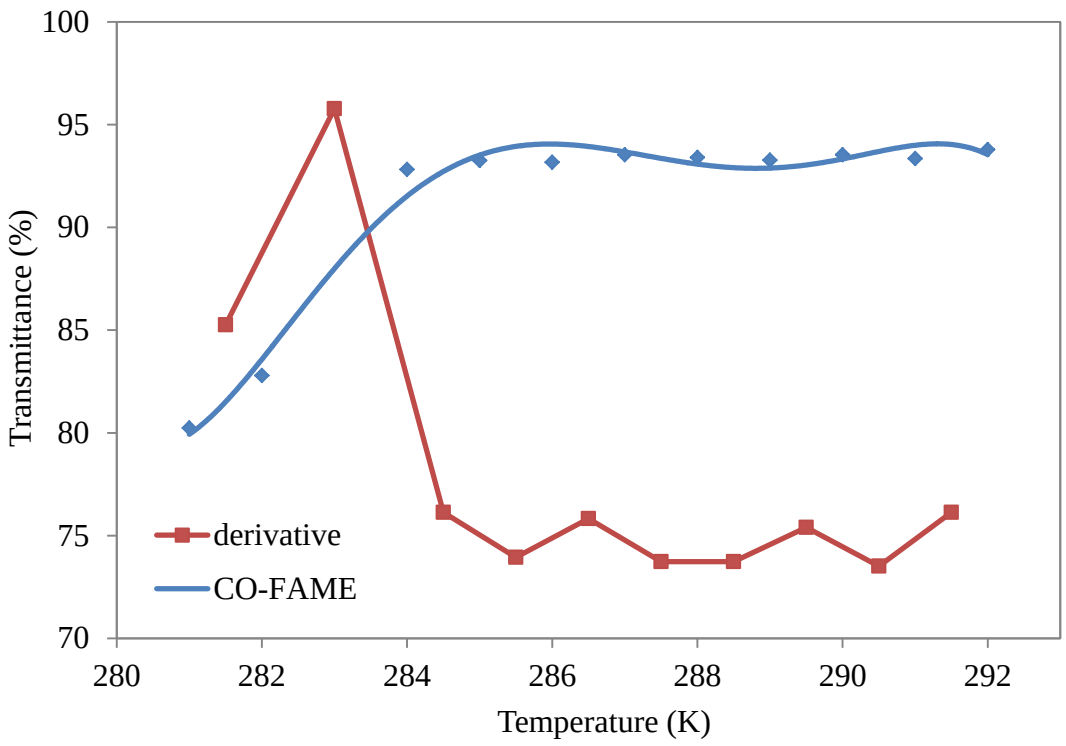


Figure 21. Plot of CO-FAME for UV-vis cloud point determination calculated by derivative of transmittance.

Table V Comparison of $CP_F$ (K) for SO-FAME with excitation wavelength of 200, 300, 400, 600 nm

| Excitation wavelength (nm) | $CP_F$ |
|---|---|
| 200 | - |
| 300 | 270 |
| 400 | 271 |
| 600 | 271 |

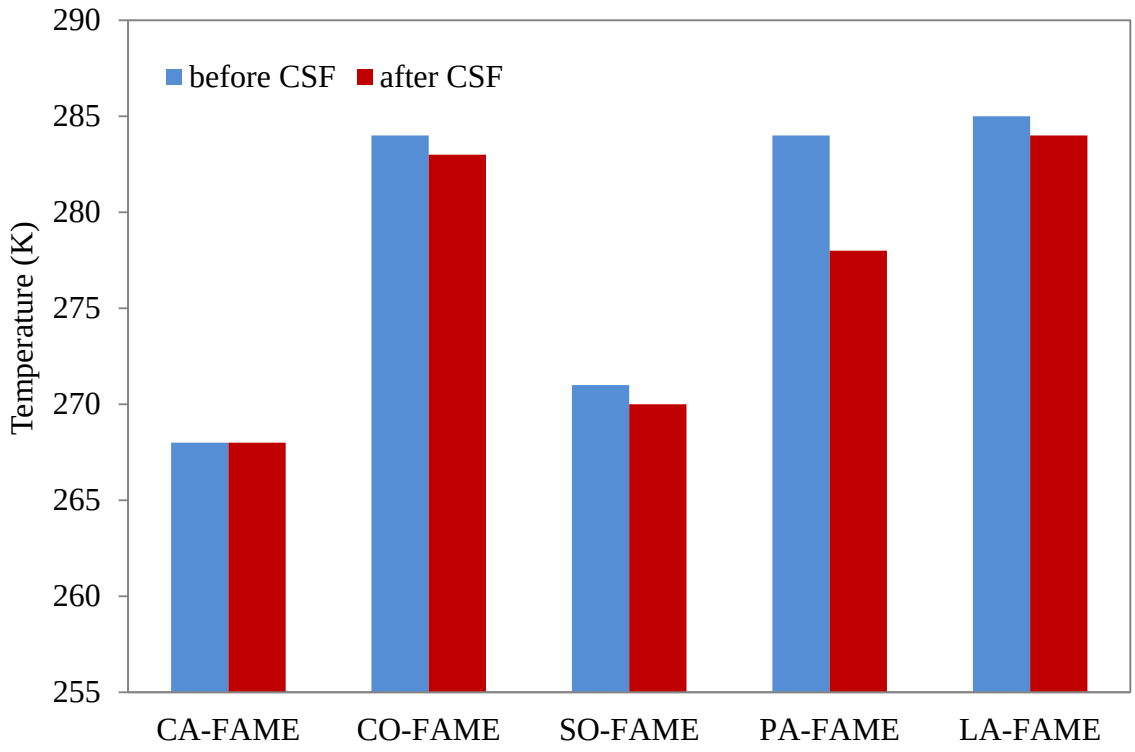


Figure 22. Comparison of $CP_F$ before and after cold soak (CSF) filtration for CA-FAME, CO-FAME, SO-FAME, PA-FAME, and LA-FAME.

Table VI Summary for CP (K) of CA-FAME, CO-FAME, SO-FAME, PA-FAME, and LA-FAME with and without additives

| | $CP_F$ | $CP_U$ | $CP_V$ |
|---|---|---|---|
| CA-FAME | 268 | 267 | 269 |
| Bio Flo | 268 | 267 | 267 |
| XC30 | 268 | 266 | 266 |
| XC40 | 267 | 267 | 266 |
| Synergy | 265 | 263 | 264 |
| CO-FAME | 284 | 283 | 282 |
| Bio Flo | 282 | 281 | 281 |
| XC30 | 281 | 280 | 280 |
| XC40 | 281 | 281 | 280 |
| Synergy | 283 | 282 | 282 |
| SO-FAME | 271 | 272 | 271 |
| Bio Flo | 271 | 271 | 270 |
| XC30 | 268 | 269 | 267 |
| XC40 | 269 | 269 | 268 |
| Synergy | 268 | 268 | 267 |
| PA-FAME | 284 | 285 | 285 |
| Bio Flo | 283 | 285 | 284 |
| XC30 | 282 | 284 | 283 |
| XC40 | 285 | 284 | 284 |
| Synergy | 281 | 282 | 282 |
| LA-FAME | 285 | 286 | 285 |
| Bio Flo | 284 | 284 | 284 |
| XC30 | 284 | 285 | 284 |
| XC40 | 285 | 285 | 285 |
| Synergy | 284 | 284 | 283 |

The RLS is applied for particles which are smaller than incident of light so Table V shows that particles formed in SO-FAME in lower temperature was greater than 200 nm because no change in the intensity was obtained with the 200 nm excitation wavelengths even when particles formed.

According to summary Table VI, slight changes in the CP were achieved using Bio Flo additives for all type of biodiesel. XC30, XC40, and Synergy additives typically decreased the CP more for samples with high in unsaturated compounds. Since Synergy is cold filter plugging point improver for used cooking oil and canola oil based biodiesel, reduction of CP for CA-FAME was observed compared with other additives. XC40 is specially formulated for canola and soybean oil based biodiesel but no significant improvement was obtained. LA-FAME had the least effect on the CP when additives were introduced. Overall, less than 5 K decrements of the CP were obtained using Bio Flo, XC30, XC40, and Synergy additives. Figure 22 shows that the cold soak filtration (CSF) could help lower the CP. Biodiesel which forms insoluble particles such as PA-FAME has a greater effect in CP by the CSF. The accuracy of the fluorometer cloud point method was analyzed by a linear regression analysis. It has the $R^2$ value of 0.9882 according to Figure 23. Therefore, the fluorometer cloud point method was comparable to the traditional visual observation method. There were slightly inconsistent results between the fluorometer and the UV-vis methods. This can be explained by the use of different cooling systems. The cooling system for the fluorometer had a smaller precision, hence kept the cell at consistent temperature with smaller fluctuations than the cooling system attached to the UV-Vis.

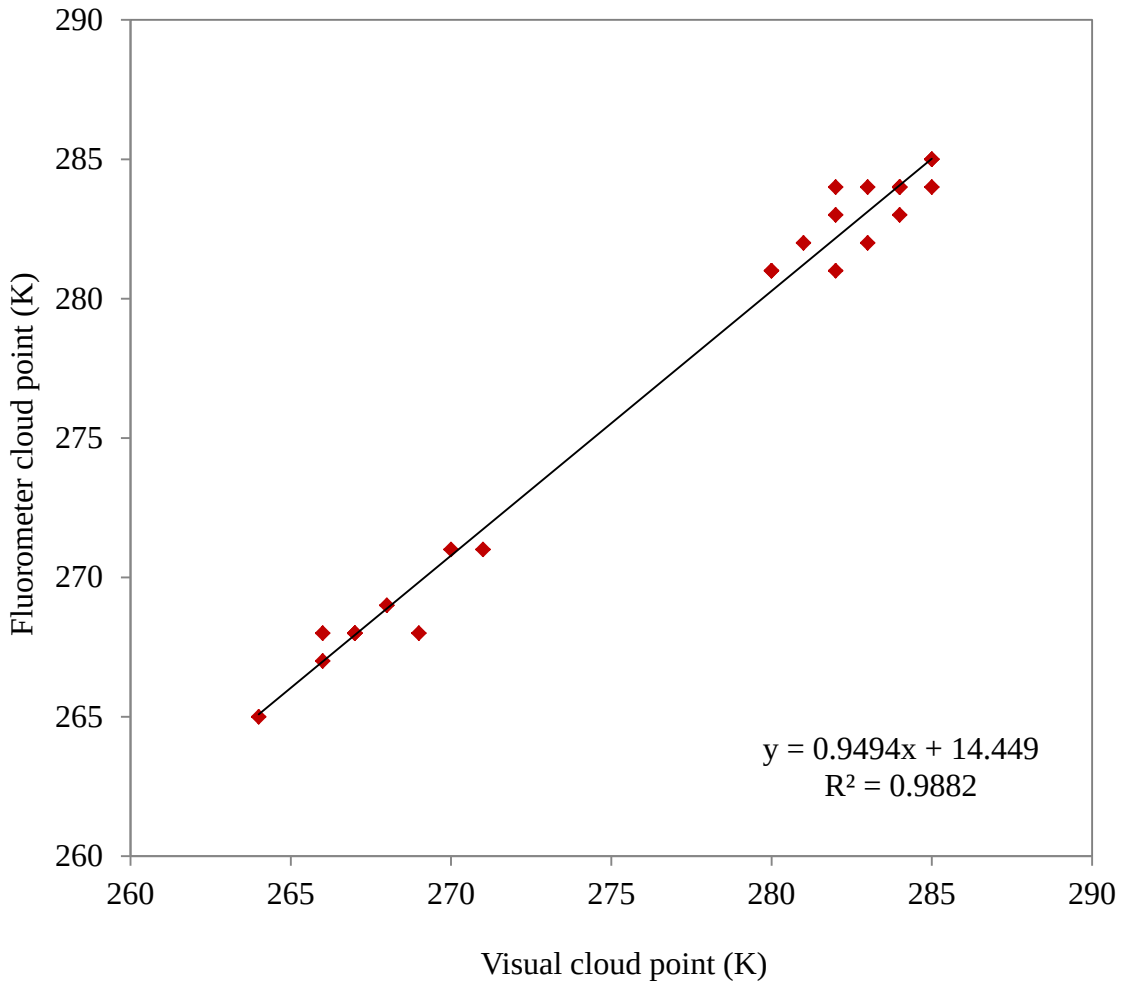


Figure 23. Linear regression analysis for fluorometer cloud point and visual cloud point.

Since a 3 mm cuvette uses smaller sample volume which requires less time to achieve constant temperature inside sample, shorter equilibrium time is predicted. Shorter equilibrium times were observed for CA-FAME, PA-FAME, and LA-FAME according to Table VII. However, CO-FAME and SO-FAME required the same amount of equilibrium time to achieve the $CP_F$. No correlation between the equilibrium time and the type of biodiesel were determined from this data. The 10 mm and 3 mm cuvettes were also employed to compare the intensity of MDAS for CA-FAME. Since CA-FAME had the $CP_F$ of 268 K, the MDAS can be predicted to be level above 268 K. However, Figure

24 indicates that the intensity of the MDAS gradually increased for the 10 mm cuvette compared with the 3 mm cuvette. A condensation was observed visually for the 10 mm cuvette at lower temperatures so a gradual increase in the intensity can be explained as the condensation.

Table VII Comparison of minimum equilibrium time (minute) to achieve $CP_F$ for CA-FAME, CO-FAME, SO-FAME, PA-FAME, and LA-FAME using 10 mm and 3 mm cuvettes

| | CA-FAME | CO-FAME | SO-FAME | PA-FAME | LA-FAME |
|---|---|---|---|---|---|
| 10mm | 5 | 20 | 10 | 5 | 8 |
| 3mm | 1 | 20 | 10 | 1 | 2 |

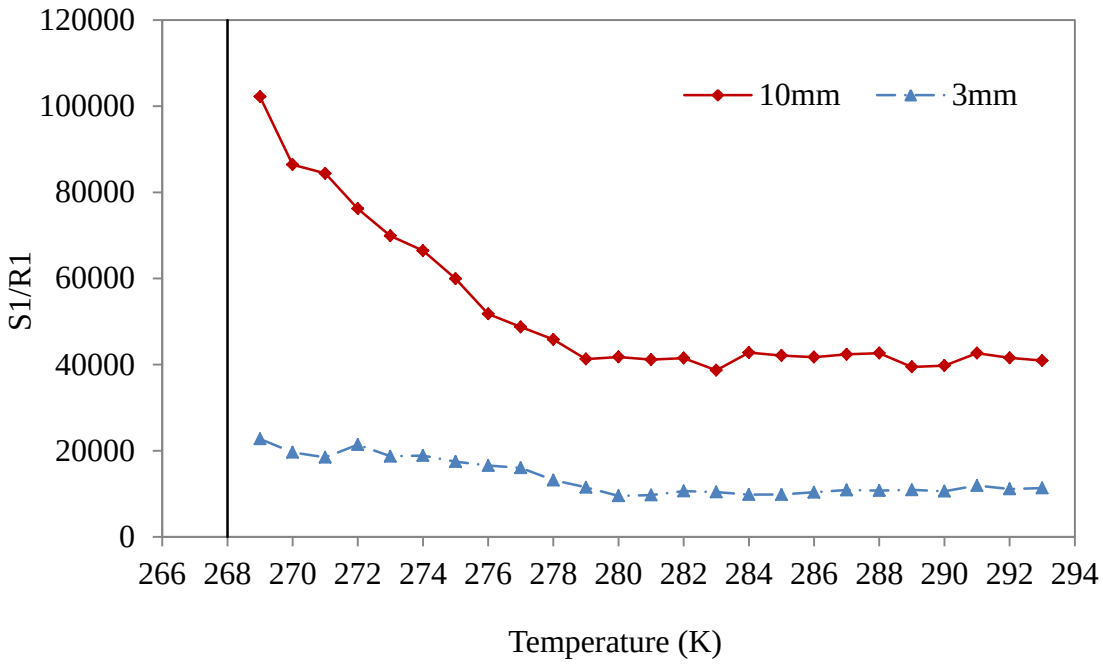


Figure 24. Comparison of intensity changes for CA-FAME minimum distinguish analytical signal using 10 mm and 3 mm cuvettes.

Multiple distinguishable freezing points (FPs) were observed from a cooling curve of CA-FAME as shown in Figure 25. The slope change caused by the latent heat of fusion occurred around 140 seconds which indicated the beginning of crystallization of some compositions (first FP). Then, the phase change of some compounds took place around 500 seconds (second FP). Finally, the eutectic compounds solidified at constant temperature between 1200 to 1350 seconds until the completion of crystallization (EP).

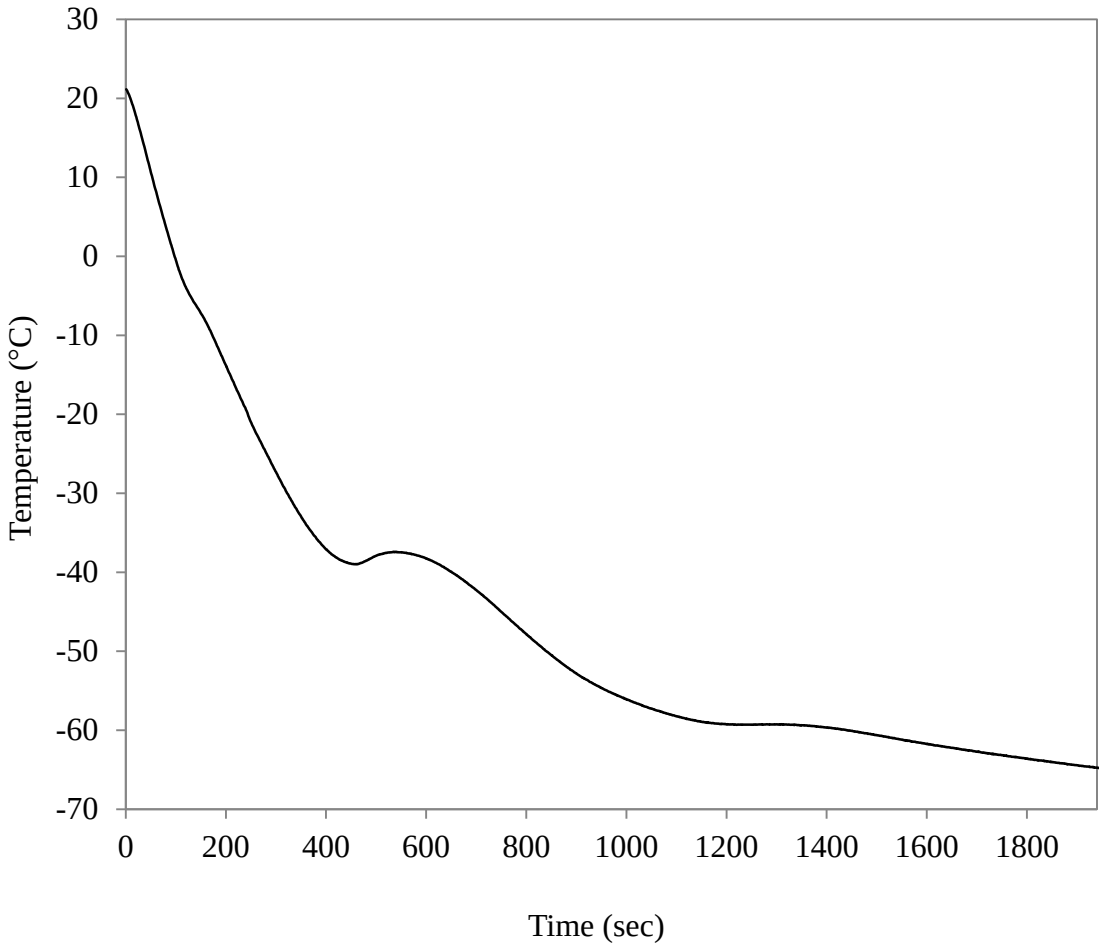


Figure 25. Cooling curve of CA-FAME.

CA-FAME was the only biodiesel showing eutectic temperature. However, identification of the eutectic compounds could not be obtained from this data. Figure 25 indicates the complete solidification because the cooling resumed after the eutectic compounds finished solidified. No relationships between the FP and additives were observed according to Figure 26. Highly unsaturated biodiesel like CA-FAME and SO-FAME took longer to solidify compared to PA-FAME and LA-FAME.

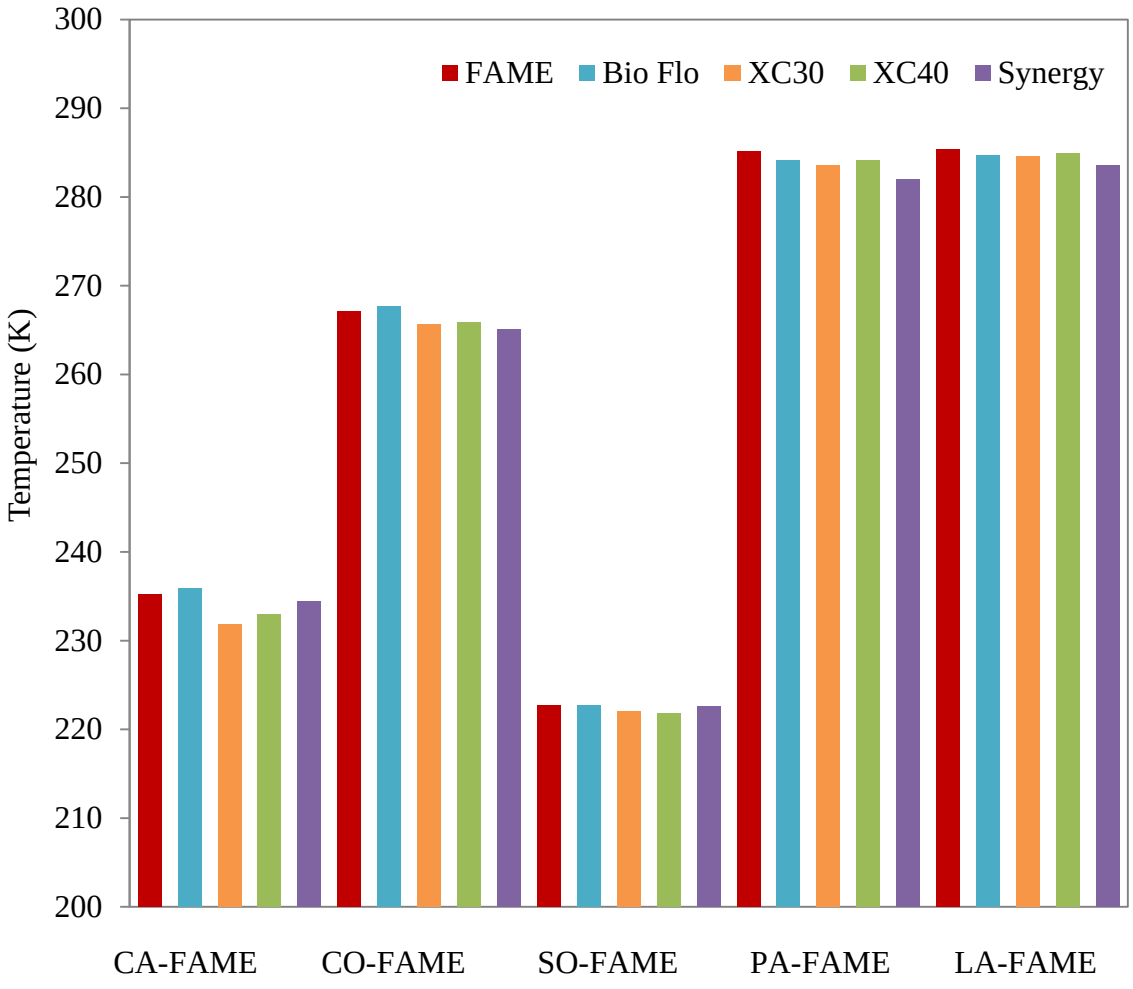


Figure 26. Freezing Point Summary for CA-FAME, CO-FAME, SO- FAME, PA-FAME, and LA-FAME and those with additives.

The first FP depression results show two different patterns depending on the length of solute according to Figure 27 and 28. Figure 27 indicates that shorter hydrocarbon of heptane, octane, and decane had linear relationships with negative slopes between the first FP. Since pure heptanes, octane, and decane have the FPs of -91, -57, and -30ºC respectively, the first FP was moving toward the freezing point of pure solute as the concentration of solute increased. On the other hand, Figure 28 shows that the solvent and solution did not have any correlations but solution with longer hydrocarbon of dodecane, tetradecane, hexadecane, and octadecane had logarithm relationships.

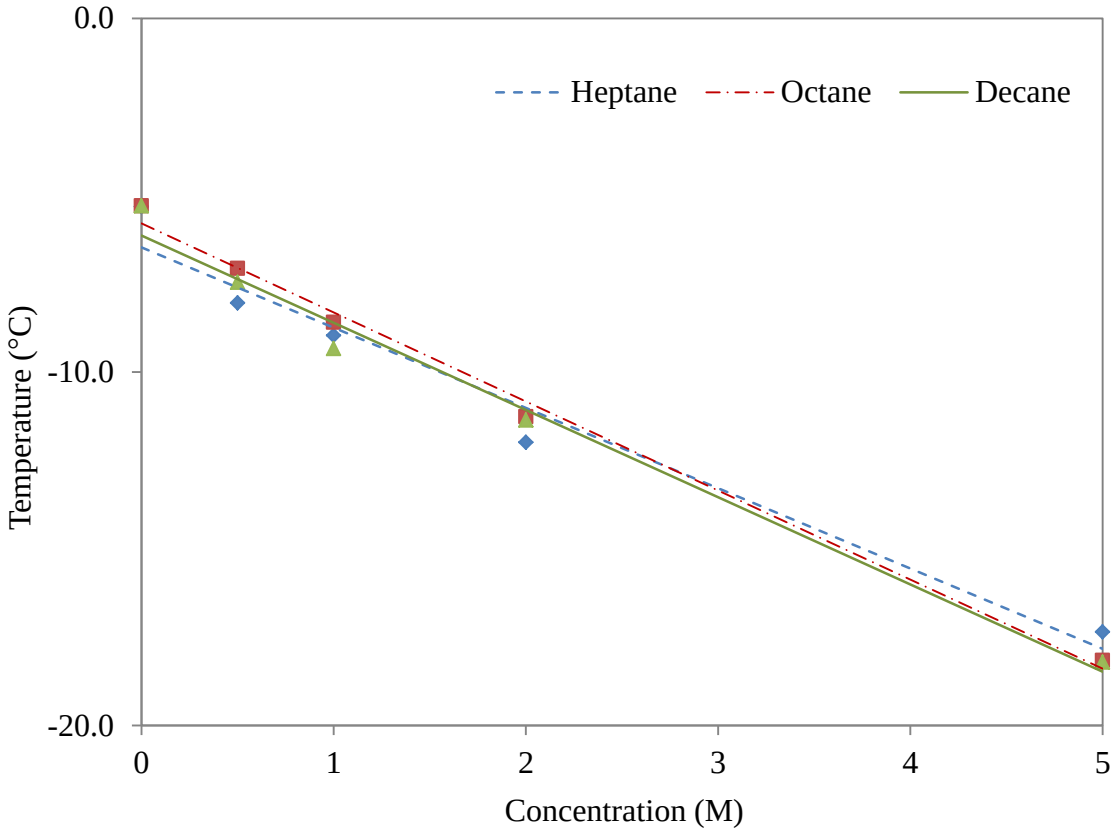


Figure 27. Change in first FP for CA-FAME with 0, 0.5, 1, 2, and 5 M of heptane, octane, and decane.

Additional of 0.5 M dodecane, tetradecane, and hexadecane decreased the first FP of CA-FAME followed by the FP depression theory but reduction in the FP could not be achieved by 0.5 M octadecane. No further depression was observed with higher solute concentrations. It can be concluded that solutes at and above 0.5 M became dominant components to control the FP. Similar phenomenon was observed in binary mixtures study by Brewer, J. and Kurata, F..[57] They concluded that the FP plot of binary mixture as a function of concentration was simple straight line when the FP of solute was similar to that of solvent but the FP started to curve as the number of carbon atoms in solute increased.

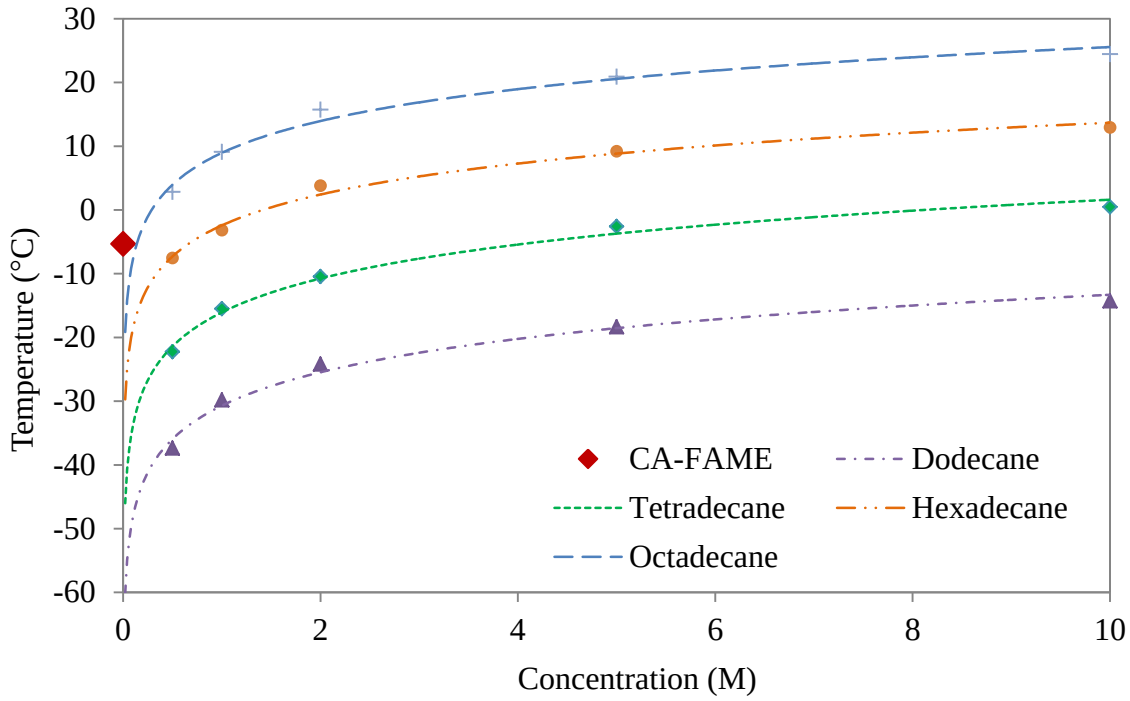


Figure 28. Change in first FP for CA-FAME with 0, 0.5, 1, 2, 5, and 10 M of dodecane, tetradecane, hexadecane, and octadecane.

The second FP for the solution with heptane and octane had the similar linear relationships as the first FP according to Figure 29. The FP of pure heptane and octane was lower than -37.7˚C which was the second FP of CA-FAME; reductions of the FP were again obtained. However, the FP of pure decane was higher than the second FP of CA-FAME so no future decrease in temperature was observed.

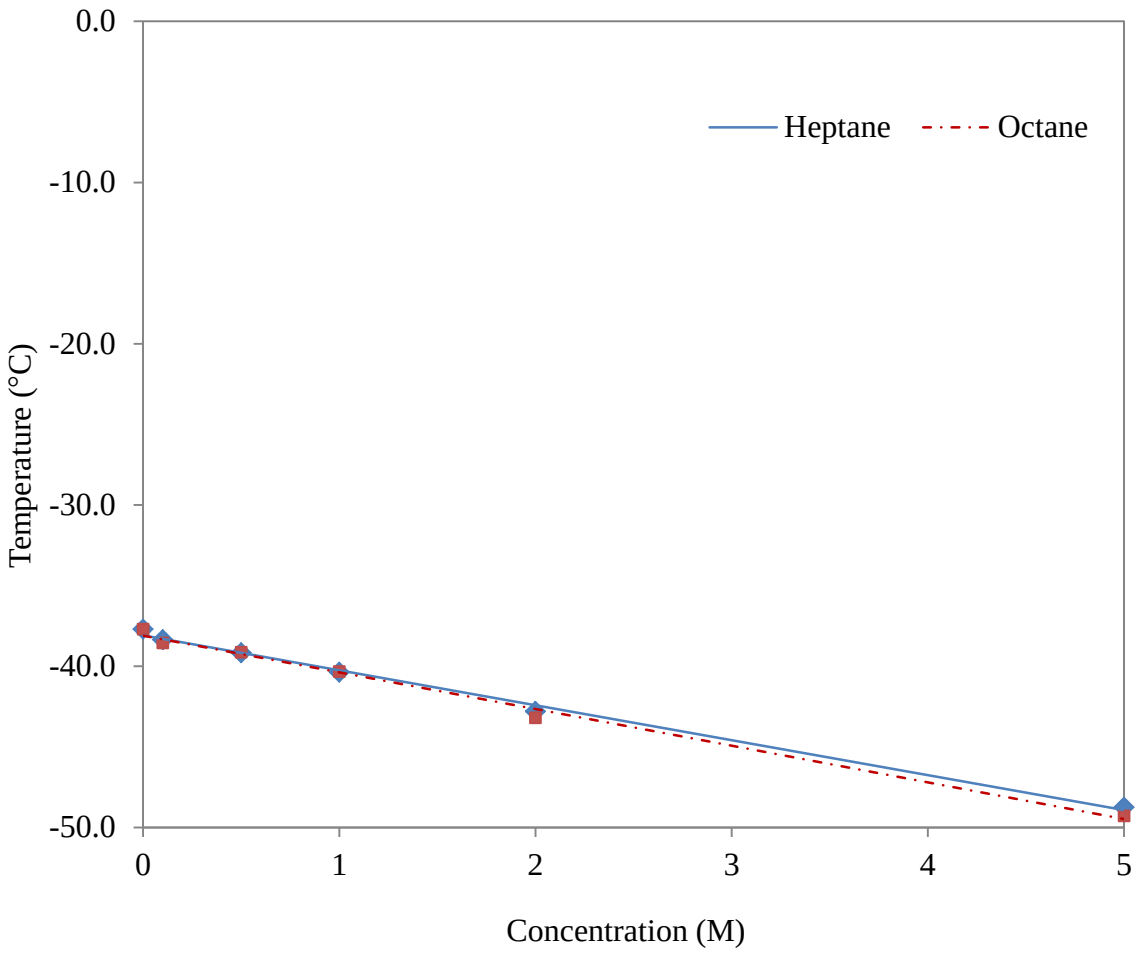


Figure 29. Change in second FP for CA-FAME with 0, 0.1, 0.5, 1, 2, and 5 M of heptane and octane.

No significant relations were seen in Figure 30 with the longer hydrocarbon solute above dodecane. All solute was successfully decreased the FP first but as the concentration of the solute increased, some decreased and some increased the FP. The FP of solutes did not show a great impact on the FP of solution. Overall, all solutions seemed to move toward the constant temperature around -40.0˚C as the solute concentration increased.

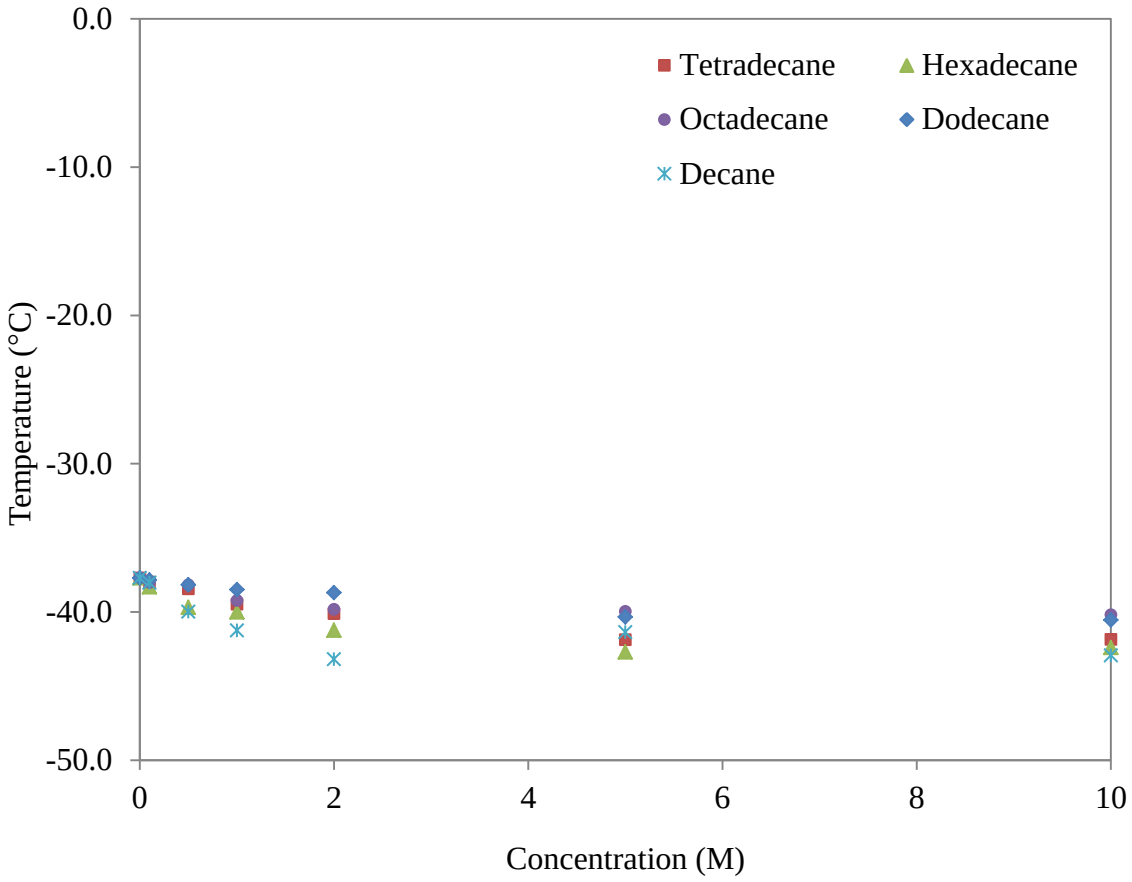


Figure 30. Change in second FP for CA-FAME with 0, 0.1, 0.5, 1, 2, 5, and 10 M of decane, dodecane, tetradecane, hexadecane, and octadecane.

# CONCLUSIONS

## Conclusion and Recommendation for Future Work

The removal of volatile byproducts was successfully achieved by the calcium-based desiccants but the calcium concentration requirement of biodiesel cannot be met due to the solubility of calcium salt in biodiesel. This issue was solved by using the combination of the calcium-based desiccants and the molecular sieves for the biodiesel purification process. This combination of desiccants reduced the calcium concentration to acceptable levels. In addition, the setting treatment method was more effective than the glass column treatment method. Therefore, the setting method with the combination of desiccants gave the best results of all. However, in order to determine whether the combination of desiccants can replace the traditional wet wash purification, further study will be necessary. Removability of other impurities such as free fatty acid and glycerol will be a good topic to examine.

The chemical and physical properties of various types of biodiesel were studied. Biodiesel was synthesized from canola oil, coconut oil, soybean oil, palm oil and lard except castor oil. In this research, new methodology for the cloud point analysis by Rayleigh light scattering was successfully developed. The 3 mm cuvette had an advantage compared to 10 mm cuvette because not only it requires small sample volume but also it gives possibility of shortened the analysis time and easier reading due to the less effect by the condensation. This work indicated that additives helped cold weather properties but the additive concentration for XC30 and XC40 used in this study created viscosity issues. Therefore, the concentration of XC30 and XC40 additives needs to

adjust in order to meet biodiesel requirements for viscosity. Moreover, additives did not change much in the chemical compositions and the freezing point of biodiesel. The results of the freezing point depression of biodiesel indicated that solutes control the freezing point even at 0.5 M therefore examining smaller concentrations may help to understand the freezing point depression of biodiesel.

# REFERENCES


1. Knothe, G. Historical perspective vegetable oil based-diesel fuels. *Inform* **2001,***12*, 1103-1107.

2. Demirbas, A. Biodiesel production from vegetable oils via catalytic and non-catalytic supercritical methanol transesterification methods. *Progress in Energy and Combustion Science* **2005,***31*, 466–487.

3. Singh, S. P.; Singh, D. Biodiesel production through the use of different sources and characterization of oils and their esters as the substitute of diesel: A review. *Renewable and Sustainable Energy Reviews* **2010,***14*, 200–216.

4. (a) Fangrui, M.; Milford, A. H. Biodiesel production: A review. *Bioresource Technology* **1999,***70*, 1-15;(b) Encinar, J. M.; Gonzalez, J. F.; Rodriguez-Reinares, A. Biodiesel from used frying oil. Variables affecting the yields and characteristics of the biodiesel. *Industrial & Engineering Chemistry Research* **2005,***44* (15), 5491-5499;(c) Fukuda, H.; Kondo, A.; Noda, H. Biodiesel fuel production by transesterification of oils. *J. Biosci. Bioeng.* **2001,***92* (5), 405-416;(d) Bozbas, K. Biodiesel as an alternative motor fuel: Production and policies in the European Union. *Renewable and Sustainable Energy Reviews* **2008,***12* (2), 542-552.

5. Demirbas, A. Comparison of transesterification methods for production of biodiesel from vegetable oils and fats. *Energy Conversion and Management* **2008,***49* (1), 125-130.

6. Canakci, M.; Gerpen, J. V. Biodiesel production from oils and fats with high free fatty acid.*American Society of Agricultural Engineers* **2001,***44* (6), 1429–1436.

7. Knothe, G. Dependence of biodiesel fuel properties on the structure of fatty acid alkyl esters.*Fuel Processing Technology* **2005,***86,* 1059-1070.

8. Chongkhong, S.; Tongurai, C.; Chetpattananondh, P.; Bunyakan, C. Biodiesel production by esterification of palm fatty acid distillate.*Biomass and Bioenergy***2007,** 31 (8),563-568.

9. (a) Dadan Kusdiana, S. S. Effects of water on biodiesel fuel production by supercritical methanol treatment. *Bioresource Technology* **2004,***91,* 289-295;(b) Ma, F.;Clements, L. D.;Hanna, M. A. The effects of catalyst, free fatty acids, and water on transesterification of beef tallow. *American Society of Agricultural Engineers* **1998,***41* (5), 1261-1264.

10. Hsu, A. F.; Jones, K.; Marmer, W. N.; Foglia, T. A. Production of alkyl esters from tallow and grease using lipase immobilized in a phyllosilicate sol-gel. *Journal of the American Oil Chemists' Society* **2001,***78* (6), 585-588.

11. Freedman, B.; Pryde, E. H.; Mounts, T. L. Variables affecting the yields of fatty esters from transesterified vegetable oils. *Journal of the American Oil Chemists' Society* **1984,***61* (10), 1638-1643.

12. M. Berrios, R. L. S. Comparison of purification methods for biodiesel.*Chemical Engineering journal* **2008,***144*, 459-465.

13. Mazzieri, V. A.; Vera, C. R.; Yori, J. C. Adsorptive properties of silica gel for biodiesel refining. *Energy & Fuels* **2008,***22* (6), 4281-4284.

14. Sohling, U.; Ruf, F.; Schurz, K. Natural mixture of silica and smectite as a new clayey material for industrial application. *Clay Minerals* **2009,***44*, 525-537.

15. Knothe, G. “Designer” Biodiesel: Optimizing fatty ester composition to improve fuel properties. *Energy & Fuels* **2008,***22* (2), 1358-1364.

16. Anand, K.; Ranjan,A.;Mehta, P. S. Estimating the viscosity of vegetable oil and biodiesel fuels. *Energy & Fuels* **2010,***24*, 664-672.

17. Alptekin, E.;Canakci, M. Determination of the density and the viscosities of biodiesel-diesel fuel blends. *Renewable Energy* **2008,***33*, 2623-2630.

18. Refaat, A. A. Correlation between the chemical structure of biodiesel and its physical properties. *Int. J. Environ. Sci. Tech.* **2009,***6* (4), 677-694.

19. Knothe, G.; Kevin, R. S. Kinematic viscosity of biodiesel components (fatty acid alkyl esters) and related compounds at low temperature. *Fuel* **2007,***86*, 2560-2567.

20. Rodrigues, J.; Cardoso, F.; Lachter, E.; Estevão, L.; Lima, E.; Nascimento, R. Correlating chemical structure and physical properties of vegetable oil esters. *Journal of the American Oil Chemists' Society* **2006,***83* (4), 353-357.

21. Chuang-Wei Chiu, L. S., GalenJ. Suppes, Impact of cold flow improvers on soybean biodiesel blend.*Biomass and Bioenergy* **2004,***27* (5), 485-491.

22. Lotero, E.; Liu, Y.; Lopez, D. E.; Suwannakarn, K.; Bruce, D. A.; Goodwin, J. G. Synthesis of biodiesel via acid catalysis. *Industrial & Engineering Chemistry Research* **2005,***44* (14), 5353-5363.

23. (a) HaiyingTang, S. S., K.Y. SimonNg, Fuel properties and precipitate formation at low temperature in soy-, cottonseed-, and poultry fat-based biodiesel blends. *Fuel* **2008,***87*, 3006-3017;(b) Wexler, R.; Levine, F.; Sadvary, D. J.; Sadler, J.; Scala, J. L. The effects of fatty acid molecular structure on the properties of bio-based fuels. In *27th army science conference*, Orlando, Florida, 2010.

24. Nascimento, R. S. V.; Soares, V. L. P.; Albinante, S.; Barreto, L. R. Effect of ester-additives on the crystallization temperature of methyl hexadecanoate. *Journal of Thermal Analysis and Calorimetry* **2005,***79* (2), 249-254.

25. Cheah Han Sern, C. Y. M., Zuriati Zakaria, The effect of polymers and surfactants on the pour point of palm oil methyl esters. *Eur. J. Lipid Sci. Technol.* **2007,***109*, 440-444.

26. Hamada, H.; Kato, H.; Ito, N.; Takase, Y.; Nanbu, H.; Mishima, S.; Sakaki, H.; Sato, K. Effects of polyglycerol esters of fatty acids and ethylene-vinyl acetate co-polymer on crystallization behavior of biodiesel. *European Journal of Lipid Science and Technology* **2010,***112* (12), 1323-1330.

27. Kazancev, K.; Makareviciene, V.; Paulauskas, V.; Janulis, P. Cold flow properties of fuel mixtures containing biodiesel derived from animal fatty waste. *European Journal of Lipid Science and Technology* **2006,***108* (9), 753-758.

28. Nubia M. R.; Angelo, C. P. The role of additives for diesel and diesel blended (ethanol or biodiesel) fuels; A review. *Energy & Fuels* **2007,***21*, 2433-2445.

29. Song, Y.; Ren, T.; Fu, X.; Xu, X. Study on the relationship between the structure and activities of alkyl methacrylate-maleic anhydride polymers as cold flow improvers in diesel fuels. *Fuel Processing Technology* **2005,***86* (6), 641-650.

30. (a) Eliassi, A.; Parach, A. Cloud points of poly(propylene glycol) aqueous mixtures at various concentrations. *Journal of Chemical & Engineering Data* **2010,***55* (9), 4010-4012;(b) Mohsen-Nia, M.; Rasa, H.; Modarress, H. Cloud-point measurements for (water + poly(ethylene glycol) + salt) ternary mixtures by refractometry method. *Journal of Chemical & Engineering Data* **2006,***51* (4), 1316-1320;(c) Alex, R. F.; Fuhr,

B. J.; Klein, L. L. Determination of cloud point for waxy crudes using a near-infrared/fiber optic technique. *Energy & Fuels* **1991,***5* (6), 866-868.

31. Standard test method for cloud point of petroleum prodcuts. In *ASTM D2500-09*, ASTM International: West Conshohocken, PA, 2009.

32. Sajith, V.; Sobhan, C. B.; Peterson, G. P. Experimental investigations on the effects of cerium oxide nanoparticle fuel additives on biodiesel. *Advances in Mechanical Engineering* **2010**, 1-6.

33. Rahman, M. S.; Guizani, N.; Al-Khaseibi, M.; Ali Al-Hinai, S.; Al-Maskri, S. S.; Al-Hamhami, K. Analysis of cooling curve to determine the end point of freezing. *Food Hydrocolloids* **2002,***16* (6), 653-659.

34. Halpern, A. M.; McBane, G.*Experimental physical chemistry: a laboratory textbook* 3rd ed.; W. H. Freeman and Company: New York, 2006.

35. (a) Hu, E.; Lai, Z.; Wang, K. Adsorption properties of the SAPO-5 molecular sieve. *Journal of Chemical & Engineering Data* **2010,***55* (9), 3286-3289;(b) Caro, J.; Finger, G.; Kornatowski, J.; Richter-Mendau, J.; Werner, L.; Zibrowius, B. Aligned molecular sieve crystals. *Advanced Materials* **1992,***4* (4), 273-276.

36. Wang, M.; Yang, J.; Wu, X.; Huang, F. Study of the interaction of nucleic acids with acridine red and CTMAB by a resonance light scattering technique and determination of nucleic acids at nanogram levels. *Analytica Chimica Acta* **2000,***422* (2), 151-158.

37. Rashid, U.; Anwar, F. Production of biodiesel through optimized alkaline-catalyzed transesterification of rapeseed oil. *Fuel* **2008,***87* (3), 265-273.

38. Predojevic, Z. J. The production of biodiesel from waste frying oils; A comparison of different purification steps. *Fuel* **2008,***87*, 3522-3528.

39. Standard test method for determination of fuel filter blocking potential of biodiesel (B100) blend stock by cold soak filtration test (CSFT). ASTM International: West Conshohochen, PA, 2009; Vol. ASTM D7501-09b.

40. O'Brien, R. D.*Fats and Oils: Formulating and Processing for Applications*. 3 ed.; CRC Press: New York, 2008.

41. Zlatica J, P. The production of biodiesel from waste frying oils: A comparison of different purification steps. *Fuel* **2008,***87* (17-18), 3522-3528.

42. Alexandre de Jesus, Ariane, V. Z. Determination of calcium and magnesium in biodiesel by flame atomic absorption spectometry using microemulsions as sample preparation. *Energy & Fuels* **2010,***24*, 2109-2112.

43. Moraes, M. S. A.; Krause, L. C.; da Cunha, M. E.; Faccini, C. S.; de Menezes, E. W.; Veses, R. C.; Rodrigues, M. R. A.; Caramão, E. B. Tallow biodiesel: Properties evaluation and consumption tests in a diesel engine. *Energy & Fuels* **2008,***22* (3), 1949-1954.

44. Standard test method for kinematic viscosity of transparent and opaque liquids (and calculation of dynamic viscosity). ASTM International: West Conshohocken, PA, 2009; Vol. ASTM D445-09.

45. Skoog, D. A.; Holler, E. J.; Grouch, S. R.*Principles of Instrumental Analysis*. 6 ed.; Thomson Higher Education Belmont 2007.

46. Long, G. L.; Winefordner, J. D. Limit of detection. A closer look at the IUPAC definition. *Analytical Chemistry* **1983,***55* (7), 712A-724A.

47. Stephen, M. A.; J. L. C.; Stephanie, N. T.; Keith, B. R. Determination of the heat of combustion of biodiesel using bomb calorimetry.*Journal of Chemical Education* **2006,***83* (2).

48. Haas, M. J.; Adawi, N.; Berry, W. W.; Feldman, E.; Kasprzyk, S.; Ratigan, B.; Scott, K.; Landsburg, E. B. Butter as a feedstock for biodiesel production. *Journal of Agricultural and Food Chemistry* **2010,***58* (13), 7680-7684.

49. Simoni M. Plentz M.; Mario R. M.;Carlos R. W.; Eid C. S.; G. E. S. L.; Masurquede de A. C.; João Inácio S.; Sandra, H. V. C. Ethanolysis of castor and cottonseed oil: A systematic study using classical catalysts.*Journal of American Oil Chemists' Society* **2006,***83*, 819-822.

50. Haiying, T.; Rhet, C. D. G.; Steven, O. S.; Simon Ng, K. Y. Formation of insolubles in palm oil-, yellow grease-, and soybean oil-based biodiesel blends after cold soaking at 4 °C.*Journal of American Oil Chemists' Society* **2008,***85*, 1173-1182.

51. Michaels, A. M.; Nirmal, M.; Brus, L. E. Surface enhanced Raman spectroscopy of individual rhodamine 6G molecules on large Ag nanocrystals. *Journal of the American Chemical Society* **1999,***121* (43), 9932-9939.

52. Guo, Z. X.; Shen, H. X. A highly sensitive assay for protein using resonance light-scattering technique with dibromohydroxyphenylfluorone-molybdenum(VI) complex. *Spectrochim. Acta, Part A* **1999,***55A* (14), 2919-2925.

53. Zhu, J.; Wang, Y.; Huang, L.; Lu, Y. Resonance light scattering characters of core-shell structure of Au-Ag nanoparticles. *Physics Letters A* **2004,***323* (5-6), 455-459.

54. Kim, J. Y.; Hwang, M. S.; Kim, Y.-H.; Kim, H. J.; Lee, Y. Origin of low dielectric constant of carbon-incorporated silicon oxide film deposited by plasma enhanced chemical vapor deposition. *Journal of Applied Physics* **2001,***90* (5), 2469-2473.

55. Chuck, C. J.; Bannister, C. D.; Hawley, J. G.; Davidson, M. G.; La Bruna, I.; Paine, A. Predictive model to assess the molecular structure of biodiesel fuel. *Energy & Fuels* **2009,***23* (4), 2290-2294.

56. Spangler, J.; Davies, E. Freezing points, densities, and refractive indexes of system glycerol-ethylene glycol-water. *Industrial & Engineering Chemistry Analytical Edition* **1943,***15* (2), 96-99.

57. Brewer, J.; Kurata, F. Freezing points of binary mixtures of methane. *AIChE Journal* **1958,***4* (3), 317-318.

I, Satomi Harada, hereby submit this thesis to Emporia State University as partial fulfillment of the requirements for an advanced degree. I agree that the Library of the University may make it available to use in accordance with its regulations governing materials of this type. I further agree that quoting, photocopying, digitizing or other reproduction of this document is allowed for private study, scholarship (including teaching) and research purposes of a nonprofit nature. No copying which involves potential financial gain will be allowed without written permission of the author.

Satomi Harada

Data

Chemical and Physical Properties of Biodiesel

Title

Signature of Graduate School Staff

Data Received